October 7, 1998 VERSION 4.0

Algorithm Theoretical Basis Document (ATBD) for the MODIS Snow-, Lake Ice- and Sea Ice-Mapping Algorithms

Dorothy K. Hall
Associate MODIS Team Member
Hydrological Sciences Branch
NASA/Goddard Space Flight Center
Greenbelt, MD 20771

Andrew B. Tait
Scientist
Universities Space Research Association
7501 Forbes Blvd., Suite 206
Seabrook, MD 20706

George A. Riggs
Scientist/Programmer
Research and Data Systems Corporation
7833 Walker Drive, Suite 550
Greenbelt, MD 20770

Vincent V. Salomonson
MODIS Team Member
Earth Sciences Directorate
NASA/Goddard Space Flight Center
Greenbelt, MD 20771

With contributions from:

Janet Y.L. Chien
Programmer/Analyst
General Sciences Corporation
6100 Chevy Chase Drive
Laurel, MD 20707

Andrew G. Klein
Scientist
Department of Geography
MS 3147
Texas A & M University
College Station, TX 77843-3147

Table of Contents

EXECUTIVE SUMMARY

Algorithms are being developed to map snow and ice cover (including ice on large, inland lakes), albedo, sea ice cover, and sea ice surface temperature (IST), using future Earth Observation System (EOS) Moderate Resolution Imaging Spectroradiometer (MODIS) data. The Level-3 products (digital maps) will provide daily and 8-day composites of global snow and lake ice cover at 500-m resolution, and sea ice cover and IST at 1-km resolution. Statistics will be provided regarding the extent and persistence of snow and ice cover at each grid cell for the Level-3 products. The snow-mapping algorithm (Snowmap) employs a Normalized Difference Snow Index (NDSI) to identify and classify snow on a pixel-by-pixel basis. The sea ice mapping algorithm (Icemap) uses both the NDSI and surface temperature to determine sea ice cover. Snowmap and Icemap employ the land/water mask and the MODIS cloud mask to define the areas of interest. Then the MODIS surface reflectance product is used as input. The usefulness of the NDSI is based on the fact that snow and ice are considerably more reflective in the visible than in the short-wave IR part of the spectrum, and the reflectance of most clouds remains high in the short-wave IR, while the reflectance of snow is low. MODIS snow and ice products will be archived at the National Snow and Ice Data Center (NSIDC) Distributed Active Archive Center (DAAC), located in Boulder, Colorado.

Validation of the Snowmap and Icemap algorithms has been and continues to be undertaken in the pre-launch time frame and will be on-going in the post-launch time frame. Current validation efforts have focused on the Sierra Nevada Mountains in California, the Upper Rhein-Felsburg Basin in the Swiss Alps, central and northern Alaska, the Bering Sea near St. Lawrence Island, and the northeastern United States. These studies show variable results, but indicate that the MODIS snow and ice algorithms perform well over a range of snow covered land surfaces and sea ice conditions. Improvements to the original prototype MODIS snow mapping algorithm have allowed more snow cover to be mapped in forests than was previously possible.

The accuracy of the MODIS snow maps will vary with land-cover type. Hence, the Snowmap algorithm has been and will continue to be tested for a variety of land covers. Error estimates have been determined from field measurements for

different land covers, and these errors are used to estimate the expected maximum monthly and annual errors in Northern Hemisphere snow mapping using Snowmap. The maximum, aggregated Northern Hemisphere snow-mapping error is expected to be about 7.5%. The error is expected to be highest (around 9-10%) when snow covers the Boreal Forest, roughly between November and April.

Sea ice extent, IST, and generalized sea ice type (snow covered sea ice and new ice) have been estimated using reflectance and emittance characteristics derived from MODIS Airborne Simulator (MAS) data over the Bering Sea. Independent validation activities in support of the Icemap and IST algorithms are planned to verify the coefficients, and modify the IST equation if necessary. In addition, dynamically-adaptive coefficients may be included to adjust for specific geographical regions, seasons, surface temperatures, or combinations of parameters to increase the accuracy of the algorithms.

The MODIS snow and ice products will be validated in relationship to EOS and non-EOS snow data sets, as well as ground observations. Focused aircraft and field campaigns have been and will be undertaken in order to validate Snowmap and Icemap. Aircraft and field experiments have been conducted in forested areas of Montana, Saskatchewan and Alaska, over prairies in Montana, tundra in Alaska, and over sea ice in the Bering and Beaufort Seas off the coasts of Alaska. The MAS has been flown in Saskatchewan, Alaska and the northeastern United States. Additional campaigns are planned to validate the snow and ice maps and IST using ground and aircraft data in the pre- and post-launch time frame.

For post-launch validation of river-basin scale areas, Landsat-7 Enhanced Thematic Mapper+ (ETM+) and EOS Advanced Spaceborne Thermal Emission and Reflection Radiometer (ASTER) data will also be used following the launch of the first EOS-AM spacecraft. For post-launch validation at the hemispheric scale, NOAA/NESDIS snow and sea ice maps will be available for comparison. NOAA National Operational Hydrologic Remote Sensing Center (NOHRSC)-derived regional maps are now available, and in the future will be available for comparison with the MODIS maps. Advanced Microwave Scanner Radiometer (AMSR)-derived snow and ice maps will be available (in 2000 and beyond).

Only in the post-launch time frame will it be possible to determine the full capabilities of the MODIS for snow and sea ice mapping because the unique combination of MODIS spectral bands has not been available on a satellite prior to MODIS. Also in the post-launch time period, and, after the launch of the EOS-PM spacecraft, the potential exists for combining MODIS, Multi-Angle Imaging Spectro-Radiometer (MISR) and AMSR data products to generate an enhanced snow product. It is envisioned that a product can be developed that will employ reflective and passive-microwave data that will permit snow extent, albedo and

depth to be mapped, thus enabling daily maps to be generated irrespective of cloud cover and darkness.

1.0 INTRODUCTION

The purpose of the MODIS snow mapping (Snowmap) and ice mapping (Icemap) algorithms is to generate global snow- and lake-ice cover products, and global sea ice-cover products from MODIS data. The Snowmap algorithm is based on ratioing techniques that have been proven to be successful at local and regional scales. Results herein show that the technique can be applied globally. Daily snow and ice maps and maximum 8-day lake ice cover, snow covered area (i.e. hemispheric snowline), and daily and maximum 8-day composited sea ice-cover and sea ice surface temperature (IST) Level-3 digital-map products will be generated in the Product Generation System (PGS) of the Earth Observation System Data Information System (EOSDIS) (Figures 1 and 2). Snow and ice products will be archived at and distributed from the National Snow and Ice Data Center (NSIDC) Distributed Active Archive Center (DAAC) at the University of Colorado in Boulder, Colorado.

The MODIS snow maps will augment the valuable record of Northern Hemisphere snow cover that was started in 1966 by NOAA (Matson *et al.*, 1986). The numerous spectral bands and superior spatial resolution of MODIS, relative to the Advanced Very High Resolution Radiometer (AVHRR), will permit an improved ability to map snow and ice. The MODIS snow cover product will be an advancement over the NOAA maps because MODIS-derived maps will provide snow maps at 500-m spatial resolution (versus 25-km resolution for the NOAA product); also, daily as well as 8-day composite maps will be produced from MODIS data. Also, the MODIS product development will be automated thus reducing or eliminating errors due to human subjectivity. Statistics concerning snow cover persistence and duration from the 8-day composites will be generated.

The sea ice maps will augment the record of sea ice cover that is produced by NOAA. Currently, there is no IST product generated on a regular basis from satellites. Therefore, the MODIS IST product will represent an important advance for the sea ice and global modeling communities.

Snowmap and Icemap will identify snow, lake ice and sea ice by their reflectance or emittance properties. Snowmap consists of a series of criteria tests and decision rules that identifies snow and lake ice, if present, in each pixel of a MODIS image. Snowmap will generate a data set of global snow cover and of ice cover on large, inland lakes at 500-m resolution. Icemap is structured in a similar fashion to Snowmap, for mapping daily and maximum 8-day composited sea ice cover globally at 1-km resolution. Also at 1-km resolution, IST will be

mapped daily and average ice surface temperature will be mapped for 8-day periods, day and night.

The basic techniques used in the snow and ice mapping algorithms are threshold-based criteria tests, the normalized difference between bands, and decision rules. Use of the ratio of a short-wave IR channel to a visible channel was determined by Kyle *et al*. (1978) and Bunting and d'Entremont (1982) to be useful for snow cover mapping, and later utilized by Dozier (1989) to map snow in the Sierra Nevada Mountains. This method is the basis for Snowmap and is also used in Icemap. The basis of the IST algorithm is the work of Key *et al.* (1997). The IST algorithm will employ the two MODIS IR channels 31 and 32, centered at approximately 11.0 and 12.0 μm.

Expected errors will be determined quantitatively in the pre-launch time frame by determining snow-mapping errors in 7 land covers (forests, mixed agriculture and forest, barren/sparsely-vegetated, tundra, grassland/shrubland, wetlands, and snow/ice). These errors will be extrapolated to the hemispheric and global scale for a rough estimate of total error in snow mapping using Snowmap over these large scales. In the post-launch time frame, use of the MODIS land-cover map will permit us to improve our error estimate, both in individual land covers and on the global scale.

Development of algorithms to map snow, lake ice and sea ice is an evolutionary process. The algorithms may change as input data and information improve, and in response to the results of validation studies. For example, the snow mapping algorithm has recently been significantly modified to more accurately map snow in forested areas. In the post-launch time frame, the full capabilities of the MODIS sensor can be utilized to optimize the derivation of snow, lake ice, sea ice cover and IST.

1.1 Experimental Objective

The snow, lake ice and sea ice products will be used to monitor the variability and trends in global snow and ice extent, and to determine duration of lake ice on large, inland lakes. Global snow cover and sea ice are important parameters in the global energy balance, and IST has a profound influence on sea ice growth, snow metamorphosis, and snow/ice melt (Key *et al*., 1997). It has been shown that global climate models (GCMs) do not simulate the present Arctic climate very well (Bromwich *et al*., 1994); thus improved measurements of global snow and ice cover and other cryospheric elements are necessary to improve modeling scenarios.

The objective of this research is to develop and implement algorithms that will map snow and ice on a daily basis, and provide statistics about the extent and persistence of snow and ice cover over an 8-day period. The Snowmap and

Icemap output products will consist of daily data and data composited to create a digital map of maximum 8-day global snow, lake ice and sea ice extent (Level-3 product). [See Appendix A for definitions of product level descriptions.] Data will be gridded in a polar-stereographic projection for the Northern and Southern Hemispheres, then cast to a sinusoidal projection for snow and lake ice cover, and retained in the polar-stereographic projection for sea ice and IST maps. IST will also be mapped daily and average IST will be mapped in 8-day composites. Snow cover in pixels that are 50% or greater snow covered will be mapped.

MODIS-derived snow and sea ice extent will also be produced at 1/4° X 1/4° resolution and will be available as input to GCMs. Also, at a typical GCM grid scale of 60 X 60 km, the 500-m resolution data will enable sub-pixel snow mapping for use in regional and global climate models. A snow cover submodel can be used to take advantage of patchy snowmelt modeling developments (Liston, 1995). From the 500-m resolution snow product, snow cover depletion curves for each model grid cell can be calculated (Glen Liston, oral communication, 1996). The generation of a methodology which directly accounts for the influence of subgrid-scale snow cover variability, within the context of regional and global climate models, is expected to improve key features of the model-simulated Earth's radiation balance and land-surface hydrology.

A consistent record of ice conditions on large inland lakes will permit studies to be done on freeze-up and break-up dates of large lakes. These data can be correlated with regional meteorological conditions and will be useful in climate-change studies. Such a record, at 500-m resolution, may also be useful to operational ice mapping for navigation. However, our planned maps are not designed for such an application because the time required to generate and distribute the EOS data following acquisition is likely to be greater than that required for operational use.

1.2 Algorithm Implementation

Expected MODIS data inputs to Snowmap and Icemap are MODIS calibrated, geolocated surface reflectances and the MODIS cloud mask. The surface reflectance product is scheduled to be available soon after launch. In addition, an ancillary land/water mask will be required. Current plans call for usage of the 1-km land/water mask being generated by the EROS Data Center in Sioux Falls, South Dakota.

Both Snowmap and Icemap are coded in sensor-specific versions for prototyping. Specific sensor versions of the algorithms are necessitated by the fact that no current instrument has all the MODIS bands or capabilities. Current instruments have band coverage over some of the regions of the electromagnetic spectrum that MODIS will cover; these are used for developing algorithm concepts. The Landsat TM and the MAS are the sensors most relevant for testing algorithms

before launch and for laying the foundation for the at-launch algorithms. However, TM views only +/-8° from nadir and has only 7 spectral bands. The MAS views +/-43° from nadir, which is close to the MODIS view angles that will be used in our algorithm (+/-45), and the MAS has 50 channels.

2.0 BACKGROUND

2.1 Remote Sensing of Snow Cover

Satellites are well suited to the measurement of snow cover because the high albedo of snow presents a good contrast with most other natural surfaces except clouds. Because of this characteristic, snow was observed in the first image obtained from the TIROS-1 weather satellite following its April 1960 launch (Singer and Popham, 1963). However, it was in the mid-1960s that snow was successfully mapped from space on a weekly basis following the launch of the ESSA-3 satellite. ESSA-3 carried the Advanced Vidicon Camera System (AVCS) that operated in the spectral range of 0.5 - 0.75 μm with a spatial resolution at nadir of 3.7 km. Using a variety of sensors, including the Scanning Radiometer (SR), Very High Resolution Radiometer (VHRR) and AVHRR sensors, snow cover has been mapped in the Northern Hemisphere on a weekly basis since 1966 by NOAA (Matson *et al.*, 1986; Matson, 1991).

The average maximum snow cover in the Northern Hemisphere occurs in the month of February and is 46.2 million km^2, based on 22 years of NOAA/NESDIS data. Work by Robinson *et al.* (1993) has shown that mean monthly snow cover in the Northern Hemisphere may have standard deviations of up to about 3×10^6 km^2, and on an annual average the standard deviation is about 1.1×10^6 km^2. Their work also shows that the standard error for monthly snow cover for the Northern Hemisphere can range from about 4 percent to about 25 percent of the monthly mean. (There is a definite seasonality in the deviations, with the greatest deviations observed for summer months and the least observed for winter months.)

Regional snow products, with 1-km resolution, are produced operationally in 3000 - 4000 drainage basins in North America by the National Weather Service using NOAA National Operational Hydrologic Remote Sensing Center (NOHRSC) data (Carroll, 1990 and Rango, 1993). Passive-microwave sensors on-board the Nimbus 5, 6, and 7 satellites and the Defense Meteorological Satellite Program (DMSP) have been used successfully for measuring snow extent at a 25- to 30-km resolution through cloud-cover and darkness since 1978 (Chang *et al.*, 1987). Passive-microwave sensors also provide information on global snow depth (Foster *et al.*, 1984). The NOAA/AVHRR and the DMSP Special Sensor Microwave Imager (SSM/I) are currently in operation. The Landsat Multispectral Scanner (MSS) and TM sensors, with 80-m and 30-m resolution, respectively, are useful for measurement of snow covered area over

drainage basins (Rango and Martinec, 1982). Additionally, Landsat TM data are useful for the quantitative measurement of snow reflectance (Dozier *et al.*, 1981; Dozier, 1984 and 1989; Hall *et al.*, 1989; Winther, 1992).

Reflectance of fresh snow is very high in the visible part of the electromagnetic spectrum, but decreases in the near-IR especially as grain size increases (O'Brien and Munis, 1975; Choudhury and Chang, 1981; Warren and Wiscombe, 1980; Warren, 1982). In addition, soot from industrial pollution becomes incorporated into the snowpack and this may decrease albedo and enhance snowmelt (Clarke and Noone, 1985; Warren and Clarke, 1985; Conway *et al.*, 1996). Both because of natural aging and other factors (e.g. soot or volcanic ash deposition), the reflectance of snow decreases over time. Fresh snow can have a reflectance (integrated over the reflective part of the spectrum) up to about 80 percent but its reflectance may decrease to below 40 percent after snow crystals metamorphose.

Snow, like all natural surfaces, is an anisotropic reflector (Salomonson and Marlatt, 1968; Dirmhirn and Eaton, 1975; Steffen, 1987). The reflectance from snow is greatest in the forward direction and is largely specular. While freshly fallen snow can be nearly a Lambertian reflecting surface, as snow metamorphoses the specular component characteristic of forward scattering increases (Dirmhirn and Eaton 1975; Steffen, 1987).

2.2 Remote Sensing of Ice on Large Inland Lakes

The formation of lake ice brings shipping and transportation on inland waterways to a standstill for several months every year in many northern areas. In addition to the impact on humans, the presence or absence of ice on lakes can have a major influence on the ecology of a region. The presence of ice can govern the viability of fish life in a lake, for example.

Lake ice formation, thickness and break-up are also key indicators of regional climate especially in data-sparse regions which characterize much of the Arctic (Palecki and Barry, 1986). Lakes that freeze each winter are good indicators of regional climate change if key parameters such as the dates of freeze-up and break-up date and maximum ice thickness are measured over a decade-scale time frame.

Some northern regions have experienced climate warming over the past few decades (or longer) as measured in the permafrost record and in meteorological records (Chapman and Walsh, 1993). Schindler *et al.* (1990) showed that air and lake temperatures in the Experimental Lakes Area of northwestern Ontario have increased by 2^{o}C, and the length of the ice-free season has increased by 3 weeks, according to 20 years of observations.

NOAA data have been used successfully to study lake ice on the Great Lakes. Because of the daily coverage of the NOAA satellites, data may be used operationally in spite of the fact that cloud-cover obscures the surface for much of the time. Ice conditions are also of interest because open water areas or large leads in the Great Lakes, for example, contribute moisture to feed major snow storms. Much work on the remote sensing of the Great Lakes has been accomplished (see Assel *et al.*, 1994).

2.3 Remote Sensing of Snow Albedo

*** Section to be included in near future ***

2.4 Remote Sensing of Sea Ice Cover

Sea ice is an important component in the global climate system. Typically overlying approximately 7 percent of the world's oceans, sea ice experiences considerable seasonal variability in both hemispheres. In the Northern Hemisphere, the total extent of sea ice varies from a minimum of about 7.8×10^6 km^2 in September to a maximum of about 14.8×10^6 km^2 in March. In the Southern Hemisphere the extent varies from about 4×10^6 km^2 in February to about 20×10^6 km^2 in September (Parkinson *et al.*, 1987). Sea ice significantly reduces the amount of solar radiation absorbed at the Earth's surface, greatly restricts exchanges of heat, mass, and momentum between the ocean and atmosphere, and affects the density structure of the upper ocean through the salt and heat fluxes associated with the freezing and melting processes. The changes in density structure at times lead to deep-water and even bottom-water formation, and the net equatorward advection of sea ice provides a transport of cold, low-salinity water out of the polar regions (Parkinson *et al.*, 1987).

Satellite remote sensing is a useful tool for mapping sea ice edges and ice concentration globally. A global year-'round record of ice-covered Antarctic and Arctic seas was acquired from the Electrically Scanning Multichannel Microwave Radiometer (ESMR) on Nimbus-5 following its 1972 launch (Zwally *et al.*, 1983; Parkinson *et al.*, 1987). Global maps of sea ice extent and concentration have been produced. The ability of passive-microwave instruments to collect data through cloud-cover and polar darkness makes them well suited for global monitoring of sea ice, but microwave instruments do not collect data on albedo or thermal-emitted energy from sea ice. Information on albedo and temperature is important during the spring-summer-autumn seasons to help analyze energy exchange of sea ice. Measurement of sea ice albedo and temperature are possible with optical sensors such as the AVHRR and Landsat TM (Lindsay and Rothrock, 1993; Key and Haefliger, 1992 and Key *et al.*, 1997) and will be possible with MODIS.

There is no ideal sensor for the comprehensive study of sea ice. Nor does a single sensor exist that is capable of measuring or monitoring the many characteristics of sea ice thought to be important to climate modeling and global change. Combinations of sensors must therefore be employed (Comiso *et al.*, 1991). The passive-microwave satellite data from the DMSP/SSM/I are obtainable daily through cloud-cover and are useful for determination of ice type and concentration. The resolution of these data, which varies from about 15-30 km, is too poor for detailed studies of ice movement and lead structure. The imaging sensors on-board the Landsat and NOAA satellites are useful for ice movement and lead orientation studies, but all-too-frequently cloud-cover intervenes to reduce the utility of the acquired data. Synthetic Aperture Radar (SAR) data are unsurpassed among remote sensors for showing lead orientation, shear zones and drift patterns throughout the year, day or night. The ERS-1 and JERS-1 satellites with SARs on-board have already provided much additional important information about sea ice since the 1991 launch of ERS-1. ERS-2 and RADARSAT data are also beginning to provide both local and regional coverage of sea ice. However, SARs do not provide global coverage on a daily basis as is possible with passive-microwave, NOAA and future MODIS sensors.

As it ages, newly-formed, smooth and thin sea ice is metamorphosed by temperature fluctuations, compressive and shear forces, surface currents and winds. In addition, the ice thickens and snow falls on top of the ice. Ridge formation and surface roughness increase with age, and the angular edges and smooth surfaces of first-year ice floes are transformed into rounded edges with hummocky, ridges and surfaces.

Because the amount of heat exchange between the ocean and the atmosphere is influenced by the thickness of sea ice, it is important to be able to distinguish first-year and multi-year sea ice using satellite data. The surface temperature of first-year and multi-year sea ice is different during the winter until the first-year ice attains a certain thickness; these temperature differences, measured by AVHRR and future MODIS sensors, should aid in the determination of ice type.

Key and Haefliger (1992) have shown that AVHRR thermal-IR data over snow covered sea ice can be used to measure ice surface temperature under clear-sky conditions. An important potential error in IST measurement occurs when ice crystal haze forms over the ice surface. Ice crystal haze can result in ice surface temperature errors of approximately 2^{o} K. Research has shown that the IST retrieval algorithm of Key and Haefliger (1992) and Key *et al.* (1997) is reliable in the Arctic, and is accurate to 0.3 - 2.1° K.

Much additional relevant research has been conducted. Only a cursory background is given in this report. Additional relevant literature is available in many sources, including Rango (1993) for snow studies, and Barry (1986) and Carsey (1992) for sea ice studies.

3.0 MODIS INSTRUMENT CHARACTERISTICS

MODIS bands covering the visible through the IR parts of the spectrum (Salomonson and Toll, 1991) will be used in the MODIS snow- and sea ice-mapping algorithms. Based on theoretical considerations and Snowmap prototyping efforts, MODIS bands 4, 6, 7, 13, 16, 20, 26, 31, and 32 (Table 1) may be used as inputs. TM and AVHRR bands corresponding to MODIS bands are also listed in Table 1 for comparison. MODIS has higher spectral resolution than the TM and AVHRR sensors. MODIS band selection for Snowmap has been largely determined by research done with comparable wavelength data from the TM sensors.

Snow typically has very high visible reflectance (Figure 3). The specifications of MODIS band response ranges are great enough that MODIS visible sensors should not saturate when observing snow. (Conversely, sensor saturation over snow in TM bands 1-3 is common; saturation in TM band 4 is less common, but may occur after a new snowfall especially in spring. Sensor saturation over snow does not occur in TM bands 5 and 7). Based on the MODIS specifications, MODIS band 4 should not saturate if snow is present; it is thus an important band for snow identification and measurement.

The wide swath (+/- 55^{o}) of the MODIS sensor will be suitable for large-area coverage. Only data from +/- 45^{o} view angles will be used for production of the snow maps because the distortions in pixel geometry and the increases in snow anisotropy at angles greater than 45^{o} are likely to adversely affect our ability to calculate snow covered area using Snowmap. Furthermore, as snow is an anisotropic reflecting surface, snow may not be mapped at non-nadir angles exactly as it is at nadir because Snowmap was designed using the TM, which is a near-nadir-viewing sensor. This is currently being investigated using MAS data [See section 4.2.3.3.].

4.0 ALGORITHM DESCRIPTIONS

4.1 Philosophy Behind Selection of Algorithms

Many different algorithms for mapping snow have been studied. A band ratio, threshold-based algorithm was selected for the following reasons:

Table 1. MODIS band centers and corresponding TM and AVHRR bands. The asterisks indicate that the MODIS band may be used as input to Snowmap and/or Icemap.

MODIS band	Center Wavelength (μm)	Spatial Res.(m)	TM band	AVHRR band
1	0.645	250		1
2	0.858	250	4	2
3	0.469	500	1	
4*	0.555	500	2	
5	1.240	500		
6*	1.640	500	5	
7*	2.130	500	7	
8	0.412	1000		
9	0.443	1000		
10	0.488	1000		
11	0.531	1000		
12	0.551	1000		
13	0.667	1000	3	1
14	0.678	1000	3	1
15	0.748	1000		2
16*	0.869	1000	4	2
17	0.905	1000		2
18	0.936	1000		2
19	0.940	1000		2
20*	3.750	1000		3
21	3.959	1000		3
22	3.959	1000		
23	4.050	1000		
24	4.465	1000		
25	4.515	1000		
26*	1.375	1000		
27	6.715	1000		
28	7.325	1000		
29	8.550	1000		
30	9.730	1000		
31*	11.030	1000	6	4/5
32*	12.020	1000		5
33	13.335	1000		
34	13.635	1000		
35	13.935	1000		
36	14.235	1000		

1) Its accuracy has been tested over a variety of surface covers relative to other derived snow cover maps; errors have been estimated for 7 different land covers [See section 4.2.3].

2) It runs automatically, without human intervention.

3) It can be employed globally.

4) It is straightforward, computationally frugal, and thus easy for the user to understand exactly how the product is generated.

While other algorithms may have greater accuracy at the regional and local scales, they do not fulfill the requirements relative to computer usage, automation and ability to map snow and ice globally.

Snow covered area from the enhanced Snowmap algorithm compares well with TM images of a forested Minnesota landscape, northern Montana forests and prairie, the Sierra Nevada Mountains, in California, Chugach Mountains, an alpine environment in Alaska, Vatnajökull ice cap, Iceland, the Brooks Range, Alaska and others. Icemap has successfully mapped sea ice on TM scenes of the southwest coast of Greenland, the Southern Ocean near Antarctica, and near St. Lawrence Island, Alaska.

Snow has strong visible reflectance and strong short-wave IR absorbing characteristics. The Normalized Difference Snow Index (NDSI) is an effective way to distinguish snow from many other surface features. Both sunlit and some shadowed snow is mapped effectively. A similar index for vegetation, the Normalized Difference Vegetation Index (NDVI) has been proven to be effective for monitoring global vegetation conditions throughout the year (Tucker, 1979 and 1986).

Other promising techniques, such as traditional supervised multispectral classifications, spectral-mixture modeling, or neural-network analyses have not yet been shown to be usable for automatic application at the global scale. They are also computationally intensive. Training or the interaction of an interpreter are required for successful application of techniques such as neural-network analysis. These techniques may progress to regional applications and possibly even global application in future years, but this evolution will not occur before 1999, when an at-launch algorithm is required to be delivered. However, in the post-launch time frame, if neural-network and/or spectral-mixture or other analysis techniques can be used to 'train' on the entire globe using MODIS data, then one of these methods might be implemented to map global snow and ice cover. If proven to improve the accuracy of the global snow-and ice-cover maps significantly, MODIS data will be reprocessed using a more advanced classification technique if the computational efficiency of the computer hardware has evolved enough to handle the increased load.

4.2 Snowmap

The snow-mapping algorithm, Snowmap (Hall *et al*., 1995; Klein *et al*., 1998), is designed to identify whether snow is present in each 500-m pixel for each orbit. A global, daily snow product will be produced. An 8-day composited snow cover product will be generated by compositing successive days of snow cover products. This will yield maximum snow extent for the 8-day period. If a pixel were snow covered on any orbit during that period, then that pixel will be mapped as snow covered even if it were snow-free on all of the other orbits during the 8-day period. Other coverage and persistence statistics will also be included to assist analysis of the data product. Summary statistics and quality assurance (QA) data will be included as metadata.

There has been much discussion concerning the optimum compositing period for the snow and ice maps (e.g. see Hall, 1995). While weekly composites would correspond with the NOAA/NESDIS maps and the NOHRSC maps, some modelers are interested in longer compositing periods, e.g., 7 days to one month. 8-day composites were chosen because this period optimizes the ground coverage from the MODIS instrument. The repeat period of the satellite is 16 days. If a researcher wants to produce a composited product for any period other than a 8-day period, from our daily product, this can be done using the daily data.

4.2.1 Normalized Difference Snow Index (NDSI)

The NDSI is useful for the identification of snow and ice and for separating snow/ice and most cumulus clouds. The NDSI is a measure of the relative magnitude of the characteristic reflectance difference between the visible and short-wave IR reflectance of snow. The NDSI is insensitive to a wide range of illumination conditions, is partially normalized for atmospheric effects, and does not depend on reflectance in a single band. The NDSI is analogous to the normalized-difference vegetation index (NDVI) (Tucker, 1979 and 1986; Townshend and Tucker, 1984). Various other techniques employing ratioing techniques have been used previously to map snow, as discussed in section 1.0. For Landsat TM data the NDSI is calculated as:

$$\text{NDSI} = (\text{TM Band 2} - \text{TM Band 5}) / (\text{TM Band 2} + \text{TM Band 5}) \qquad [\mathbf{1}]$$

Pixels that are approximately 50% or greater covered by snow have been found to have NDSI values ≥ 0.4 in our testing of a TM scene of the Sierra Nevada, California. Since water may also have an NDSI ≥ 0.4, an additional test is necessary to separate snow and water. Snow and water may be discriminated because the reflectance of water is <11% in TM band 4. Hence, if the reflectance of TM band 4 >11%, and the NDSI ≥ 0.40, the pixel is initially considered snow covered.

These NDSI thresholds have been verified from detailed analysis of numerous TM scenes, comparisons with supervised-classification techniques and comparison of a Snowmap-derived map of the 10 May 1992 TM scene of the Sierra Nevadas with a snow map derived from Rosenthal and Dozier (1996).

Pure snow has a high NDSI but NDSI decreases as other features are mixed in a pixel. Snow in mixed pixels has an NDSI that is less than that for pure snow. An example of this can be seen in Figure 4, showing snow, snow in forest, and pure forest samples from TM data covering Glacier National Park, Montana. Pure snow can be distinguished by its high NDSI value. Samples obtained from dense forests from the same location in Glacier National Park were extracted from a late-summer TM scene (3 September 1990) and from a late-winter TM scene (14 March 1991), and are labeled 'forest summer' and 'forest winter,' respectively in Figure 4. The effect of snow cover on the NDSI of forest is evident in these samples.

In forested locations, many snow covered pixels have an NDSI lower than 0.4. To correctly classify these forests as snow covered, a lower NDSI threshold is employed. The normalized difference vegetation index (NDVI) and the NDSI are used together in order to discriminate between snow-free and snow covered forests. Forested pixels have higher NDVI values compared with non-forested pixels. Thus by using the NDSI and NDVI in combination, it is possible to lower the NDSI threshold in forested areas without compromising the algorithm performance in other land covers.

The NDSI-NDVI field is designed to capture as much of the variation in NDSI-NDVI values observed in the snow covered forests as possible while minimizing inclusion of non-forested pixels (Figure 5). It was designed to include forest-covered pixels that have NDSI values lower than 0.4, yet have NDVI values lower than would be expected for snow-free conditions (Klein *et al.,* in press). Last, a threshold of 10% in TM band 2 was used to prevent pixels with very low visible reflectances, for example black spruce stands, from being classified as snow as has previously been suggested (Dozier, 1989).

To map snow cover following the MODIS launch, Snowmap will employ at-satellite reflectances in MODIS bands 4 and 6 to calculate the NDSI. A pixel will be mapped as snow if the NDSI value is ≥ 0.4 and the reflectance in MODIS band 2 is >11%. However, if the MODIS band 4 reflectance is <10%, then the pixel will not be mapped as snow even if the other criteria are met. In addition, MODIS bands 1 and 2 will be used to calculate NDVI to permit mapping snow in forests. If a pixel has NDSI and NDVI values within an irregular polygon as determined from canopy-reflectance modeling (Figure 5), it is mapped as snow covered.

4.2.2 Use of Reflectances for Calculation of NDSI in the Prototype Algorithm

In the prototype Snowmap algorithm, which employs TM data, at-satellite reflectance, r, is calculated as shown below (Markham and Barker, 1986):

$$r = (\pi L\lambda d^2) / (ESUN\lambda \cos\theta_s) \quad [2]$$

where:

- $L\lambda$ is calibrated radiance
- d is Earth-Sun distance
- $ESUN\lambda$ is mean solar exoatmospheric irradiance
- θ_s is SZA

The Earth-Sun distance and ESUN can be obtained from a look-up table. For prototype efforts, we are assuming the Earth-Sun distance to be constant at 1.0 Astronomical Unit. For the prototype algorithm, the SZA of the TM scene center is used for each pixel. The operational MODIS algorithms will omit this step because MODIS reflectance product will be the input.

Equation 2 assumes that the surface being measured has isotropic reflectance properties even though this is not the case for snow, and other natural features. Thus, errors in calculation of reflectance due to the anisotropy of snow and ice may result. Such errors will likely be greater at larger angles off nadir. Also, as snow ages, its anisotropy increases. Additionally, errors in precise reflectance value due to anisotropy related to topographic variability will be inherent in the data [see section 4.2.3.3].

4.2.3 Estimate of Global Errors in Snow Mapping with Snowmap

It is recognized that Snowmap will perform better in some land covers than in others. Specifically, in tundra and prairie areas, and over large lakes, the errors in snow mapping will be very low. Results using the Snowmap algorithm with TM and MAS data over these areas show 100 percent snow cover was mapped when they were known by field measurements to be 100 percent snow covered. In forested areas, errors may be much larger.

An estimate of the errors inherent in using Snowmap in different land covers has been made using data from focused field and aircraft missions, for example: agricultural (e.g. in the upper midwest of the U.S.), alpine (e.g. Glacier National Park, Montana), forest (e.g. the Boreal Forest in Saskatchewan), prairie (e.g. the Great Plains in eastern Montana) and tundra (e.g. the North Slope of Alaska) (Hall *et al.*, 1998). Errors have been determined for the following 7 land covers: forests, mixed agriculture and forest, barren/sparsely-vegetated, tundra, grassland/ shrubland, wetlands, and snow/ice. These land covers were selected

because they cover a wide range of conditions encountered in snow covered parts of the Earth.

The maximum expected MODIS snow-mapping errors for these 7 land-cover types are 15% for forests, 10% for mixed agriculture and forest, and 5% for other land-covers (Hall *et al.*, 1998). Estimating snow cover is most difficult in forests, because the trees partially or completely conceal the underlying snow. These errors were used to estimate the expected maximum monthly and annual errors in Northern Hemisphere snow mapping using Snowmap. The maximum monthly errors are expected to range from 5-9% for North America, and from 5-10% for Eurasia. The maximum, aggregated Northern Hemisphere snow-mapping error is expected to be about 7.5%. The error is expected to be highest (around 9-10%) when snow covers the Boreal Forest, roughly between November and April. These error estimates will be refined in the post-launch time frame, when it will be possible to use the MODIS global snow cover data and the MODIS at-launch land-cover product to identify classes of land cover globally.

Two non-EOS datasets were used to determine the above errors. 1) The 1-km IGBP digital land-cover maps of North America and Eurasia were used to identify the 7 cover types discussed above (there are 17 land covers in the IGBP map). 2) The average monthly snowline positions were obtained from the NOAA National Environmental Satellite, Data and Information Service (NESDIS). The snowline positions were registered to the land-cover maps and the percent of each of the 7 land covers north of the continental snowline was calculated monthly for North America and Eurasia. Snowmap errors derived from each of the land covers from aircraft experiments were extrapolated to the continental scale.

4.2.3.1 Mapping Snow in Densely-Forested Areas

A significant limitation in mapping the extent of snow cover occurs in situations of mixed pixels where snow cover is obscured by dense forest cover. The snow covered forested landscape is actually never completely snow covered because the tree branches, trunks and canopies often do not get or stay snow covered. Often, in boreal forests, snow that falls on the coniferous tree canopy will not stay on the canopy for the entire winter due to sublimation. Thus, even in a continuously snow covered area, much of the forested landscape will not be snow covered. It may be very difficult, even with field measurements and high-resolution air photos, to determine what percentage of the area is snow covered. Additionally, when viewing at off-nadir angles such as the angles up to $\pm 45^\circ$ that we plan to use with the MODIS sensor, the tree branches, canopies, etc., will obscure even more of the snow than when viewing at near-nadir angles [see section 4.2.3.3].

Much of the Earth's land surface is covered by dense forests. The boreal forest, the forest that stretches across the northern part of North America and Eurasia, is a prime example. Snow accumulates to greater depths and melts later in the spring in the boreal forests than in adjacent tundra or prairie areas (Foster *et al.*, 1991). Though the boreal forests are always snow covered in the winter, within dense forests, snow that falls onto the ground through the canopy may not be visible from above. Some snow stays in the tree canopy and may thus be visible, but the snow often does not stay in the canopy during the entire winter. Snow in trees often sublimates before falling to the ground. Even with passive-microwave sensors, wherein microwave emission is measured, snow under a tree canopy is often not detected (Hall *et al.*, 1982; Foster *et al.*, 1991).

Comparison of results from snow mapping using TM data, and forest-cover classification was undertaken as part of MODIS pre-launch validation activities and in connection with the Boreal Ecosystem Atmosphere Study (BOREAS). The southern BOREAS study area in southern Saskatchewan, including Prince Albert National Park, consists of mixed deciduous and coniferous trees and stands consisting of predominately deciduous or coniferous trees. Several lakes are located in the test site. The at-satellite radiances of the five BOREAS Landsat TM scenes (Table 2) were converted to at-satellite reflectances following the procedure described in Markham and Baker (1986).

The TM data were registered to a forest-cover map developed using 6 August 1990 TM imagery of the BOREAS study area by Forrest Hall at NASA/GSFC (Hall *et al.*, in press). Registration of the forest-cover map to the Snowmap maps derived from the TM scenes enabled us to ascertain, quantitatively, the influence of different types of vegetation on snow mapping in this mixed forest.

A relatively simple canopy reflectance model for discontinuous canopies (GeoSAIL), was used to determine the fraction of sunlit crown, sunlit background, shadowed crown, and shadowed background within a forest stand. It was also used to model the crown reflectances and the transmittance through the canopy. Reflectances for the sunlit snow were calculated using the Wiscombe and Warren (1980) model and the reflectances of the other components were taken from direct measurements. The objective of the study was to estimate how the presence of snow on the forest floor would alter the reflectance of a forest stand.

The primary change in reflectance occurs in the visible wavelengths as snow has a much higher visible reflectance than soil, leaves, or bark. Depending upon the vegetation type, snow may also cause a decrease in the mid-infrared reflectance of the stand. This behavior is captured in the NDSI. In addition, the reflectance in the visible will often increase with respect to the near-infrared reflectance. This change lowers the normalized difference vegetation index (NDVI). Therefore, taken together the NDVI and NDSI provide a strong signal that can be exploited to classify snow covered forests (Klein *et al.*, in press). Figure 5 shows

Table 2. Acquisition date, path, row and solar zenith angles (SZA) of the Landsat TM scenes of the BOREAS Southern Study Area used in this study.

Acquisition Date	Path	Row	SZA
8/6/90	37	22	42.1
1/18/93	37	22	77.9
2/6/94	37	22	73.6
3/29/95	37	22	55.9
9/21/95	37	22	57.4

the additional criteria field for snow covered forests derived from TM observations and the GeoSAIL model (shown in gray). Pixels falling in this field are considered to be snow covered.

One additional problem occurs in detection of snow under certain forest types. Many forest types, most notably black spruce, have very low reflectances in the 1.6 μm wavelength region (TM band 5). These low reflectances cause the denominator in the NDSI to be quite small, and only small increases in the visible wavelengths (e.g. TM band 2) are required to make the NDSI value high enough to classify a pixel as snow. For instance, if the short-wave infrared reflectance in 5%, then it may only take a visible reflectance of 12% for the NDSI to exceed 0.4. This problem is exacerbated when the NDSI-NDVI threshold is employed, as lower NDSI values will be classified as snow. To limit errors of commission, a visible threshold is used to prevent pixels with very low visible reflectances from being classified as snow as has previously been suggested by Dozier (1989). Here a threshold of 10% in TM band 2 was used. Landsat TM band 2 was selected over TM band 1 because the effects of Rayleigh scattering are greater at shorter wavelengths.

4.2.3.2 Snow / Cloud Discrimination

We will rely on the cloud-masking product, developed by Paul Menzel, Steve Ackerman and others at the University of Wisconsin, to map clouds and distinguish clouds and snow. Close coordination with that group will ensure a good result. For example, we held an aircraft and field experiment jointly with the University of Wisconsin cloud-masking group, in January and February 1997. Snow, lake ice and cloud masking was the focus of the experiment [see section 5.1.1.5]. The MAS was the primary sensor on board.

For the prototype algorithms, snow/cloud-discrimination techniques are based on differences between cloud and snow/ice reflectance and emittance, (Figure 3). Clouds are highly variable and may be detected by their generally-high reflectance in the visible and near-IR parts of the electromagnetic spectrum

(Rossow and Garder, 1993), whereas the reflectance of snow drops in the short-wave infrared part of the spectrum.

While the NDSI can separate snow from most obscuring clouds, it does not always identify or discriminate optically-thin cirrus clouds from snow. For this, MODIS channel 26, with the band center located at 1.375 μm will be used if necessary. At that wavelength, cirrus clouds are very strong absorbers, a property that may separate them from other features, including snow (Gao *et al.*, 1993). Cirrus clouds may also be detected by brightness temperatures and differences in brightness temperature at 8.55, 11.0, and 12 μm (King *et al.*, 1992). Channel 26 may be too sensitive to the presence of optically-thin cirrus clouds and thus preclude snow-mapping through thin cirrus. Analyses of TM and MAS data show that Snowmap can map snow under cirrus clouds at least some of the time. Investigation of the utility of channel 26 for use in Snowmap and Icemap will not be feasible until the post-launch time frame because the 1.375 μm channel is not available on the MAS. Since this is primarily a cloud-masking task, we will work with the MODIS cloud-masking group to accomplish this.

4.2.3.3 Variation of Reflectance due to Sensor View Angle

At the off-nadir view angles, tree canopies (both the defoliated stems from the deciduous trees, and the needles from the coniferous trees), may prevent snow under the canopies from being mapped by the Snowmap. Once MODIS has been launched and several months of data have been received, it will be possible to investigate this effect fully. At present, there is insufficient data from the MAS to determine a relationship between snow mapped by Snowmap and view angle.

Snow anisotropy may also result in some errors when mapping snow at larger view angles. Snow is not a Lambertian reflector and tends to reflect more in the forward direction, especially when the snow is aged. The increase in forward scattering with snow age is also greater in the near infrared relative to the visible. This may have an effect on the NDSI. At view angles greater than around 30° off nadir, the reflectance may differ slightly with that at nadir, as the amount of reflected solar irradiance will vary with view angle due to the anisotropy of snow. Preliminary results suggest that the change is only slight, however further investigation of this effect is required once MODIS data are available.

4.3 Snow Albedo

*** Information on the snow albedo product will be added in the near future ***

4.4 Lake Ice

The lake ice product will be produced along with, and as part of, the snow cover product. Ice will be mapped in the following large inland water bodies: Lake Superior, Lake Michigan, Lake Erie, Lake Huron, Lake Ontario, Great Bear Lake, Great Slave Lake, Lake Winnipeg, Lake Athabaska, Lake of the Woods, Lake Sakami, Lake Nipigon and Reindeer Lake in North America; Lake Vanern, Lake Ladoga, Lake Baikal, Lake Peipus, Lake Balkhash and Onega Lake in Eurasia.

4.5 Icemap

4.5.1 Development of Icemap

Icemap is designed to identify whether sea ice is present in each 1-km pixel for each orbit and to calculate the IST. Daily and 8-day composited sea ice extent will be produced in the Product Generation System (PGS). If sea ice is present in any pixel on any day during the 8-day compositing period, that pixel will be considered to be ice covered. Icemap is designed to run automatically.

Land and clouds will be masked before Icemap is run. Criteria tests and decision rules for identifying sea ice are modified versions of those used for Snowmap. The IST algorithm is used in conjunction with the Icemap algorithm to map sea ice during the day and night throughout the year.

4.5.2 Detection of Sea Ice

Measurements collected by researchers over the range of 0.4-2.4 μm show that the albedo of sea ice changes over the seasons (Grenfell and Perovich, 1984). Snow covered sea ice has albedo characteristics similar to snow, thus logic similar to that used to identify snow cover can be used to identify snow covered sea ice.

As snow melts on sea ice, the albedo decreases across all wavelengths (Grenfell and Perovich, 1984). Open ocean typically has a very low albedo, in contrast to the highly-reflective sea ice. Some types of sea ice, such as grease ice, however, may be difficult to identify with such criteria tests because they lack sharp contrast with open ocean.

Characteristics of areal extent, albedo, thickness of sea ice, ice margins, leads, ice types, motion and concentration, are important to measure as they may be used in energy-balance models (e.g. Barry, 1986). The primary contribution of the MODIS sea ice algorithm to the study and monitoring of sea ice will be the ability of MODIS data to provide some ice information at high spatial resolution (1 km) to augment the data provided by passive- and active-microwave sensors,

and to map IST. Additionally, the ability to measure surface temperature in the winter, using MODIS data, should aid in the determination of ice type, and will be useful for estimating radiative and turbulent heat fluxes for large-scale climate studies.

The MODIS sea ice algorithm identifies sea ice by its reflectance characteristics in the visible and near IR and its sharp contrast to open water. The algorithm also estimates the IST, which is used as an additional discriminatory variable for the identification of sea ice cover. The darkness of polar winters will be a limiting factor in the use of visible channels. Cloud cover in the central Arctic Basin will be a limiting factor in mid-summer (Grenfell and Perovich, 1984) especially in the daily maps. Because the 8-day composite maps will be developed, it is expected that sea ice can be mapped during the spring, summer and autumn when the greatest changes are taking place in the extent and movement of sea ice. Winter sea ice mapping may be possible if the cloud-masking algorithm works well in polar darkness.

Snow covered sea ice is determined using the following criteria. If the NDSI (using MAS channels 1 and 10) ≥ 0.4 and the visible reflectance (using MAS channel 1) > 0.11, then the pixel contains snow covered sea ice. These criteria are the same as used by Snowmap. Relatively thin sea ice (< 10 cm, with no snow cover) which has a lower albedo and which may not be detected using the NDSI, is identified using the difference between ice surface and sea surface temperature (Riggs *et al.*, in press). Details of the IST algorithm follow this section.

The determination of thin sea ice is made in two steps. First, if the difference of surface temperature at 11.0 and 12.0 μm (using MAS channels 45 and 46) is small, then a clear atmosphere may be assumed (Key et al., 1997). Second, given this assumption the surface temperature may be estimated directly from the observed brightness at 11.0 μm, adjusted to the assumed emissivity of the surface. Sea water emissivity is assumed to be 0.985 (Comiso, 1994). Using data from MAS images near St. Lawrence Island, Alaska, collected in April 1995, the mean sea water temperature is estimated to be 271.6 K. Sea ice is then identified as any pixel with a surface temperature less than or equal to the freezing point of sea water (a freezing point of 271.4 K is used based on direct estimates of open water and ice).

Sea ice cover derived from the two methods (NDSI and IST) are compared to show where they agree and disagree. From these comparisons, compound relational tests are used to produce maps where sea ice is identified by both methods, one method but not the other, and by neither method (Riggs *et al.*, in press). Using these maps, some information can be derived regarding the condition of the sea ice, in particular whether the ice is snow covered or whether it is relatively thin.

4.5.3 Ice Surface Temperature (IST) Algorithm

IR bands (MODIS bands 31 and 32) will be used for mapping sea ice surface temperature and, together with the NDSI, for estimating sea ice extent. The surface temperature of open water is > 271.4 K while the surface temperature of saline ice is ≤ 271.4 K. This value was determined from estimates of open water and ice obtained from MAS images in the Beaufort Sea, near St. Lawrence Island, Alaska.

The basis of the MODIS IST algorithm is the work of Key *et al*. (1997). Key *et al*. (1997) state that the demonstrated accuracy of the algorithm is sufficient for most climate process studies. The major caveat with the algorithm is that it is applicable only to clear-sky conditions; inadequate cloud masking may result in significant error in estimating the IST. The heritage of the technique is Key and Haefliger (1992) with substantiation of robustness and accuracy by later work (Key *et al*., 1994; Yu *et al*., 1995; Lindsay and Rothrock, 1994; Massom and Comiso, 1994).

Key and Haefliger (1992) used the following equation to determine IST for snow covered sea ice in the central Arctic under clear sky conditions.

$$IST = a + bT_{11} + cT_{12} + d[(T_{11} - T_{12})\sec\theta] \qquad [3]$$

T_{11} -- brightness temperature °K in AVHRR band 4 (11 µm)
T_{12} -- brightness temperature °K in AVHRR band 5 (12 µm)
θ -- scan angle from nadir
a, b, c, d -- empirically-determined coefficients for atmospheric effects, notably humidity.

Key *et al*. (1997) used the equation

$$IST = a + bT_{11} + c(T_{11} - T_{12}) + d[(T_{11} - T_{12})(\sec\theta - 1)] \qquad [4]$$

where all variables are defined as in [3] except that the coefficients (a, b, c, d) are defined for temperature ranges of

$T_{11} < 240K$
$240K < T_{11} < 260K$
$T_{11} > 260K$.

Equation [4] given by Key *et al*. (1997) is reported by them to be superior to that of [3]. Linking the coefficients to temperature ranges also provides greater flexibility in application of the algorithm (Key *et al*., 1997). Equation [4] is suitable for use with MODIS thermal data.

MODIS Level 1B data for the thermal IR channels (31 and 32) will be generated and archived as radiance data. The radiance data can be converted to brightness temperature by inversion of Planck's equation.

Key *et al*. (1994) used an inversion of Plank's equation with an emissivity term;

$$T = c_2 v \ / \ \ln(1 + ((\varepsilon c_1 v^3)/E)) \qquad [\mathbf{5}]$$

$c_1 = 1.1910659 * 10^{-5}$ mW m^{-2} sr cm^{-4}
$c_2 = 1.438833$ cm °K

v = central wavelength cm^{-1}
E = radiance from sensor mW m^{-2} sr cm^{-4}
T = °K
ε = emissivity

Equation [4] can then be applied to determine IST.

4.5.4 Ice/Cloud Discrimination

The IST algorithm (Equation 4) is only valid for clear-sky conditions. Any cloud contamination may cause significant errors in calculation of IST. The MODIS cloud masking product will be utilized to identify clear sky conditions; only pixels with a 95% or greater probability of being unobstructed by cloud will be considered. Other pixels will be identified as cloud contaminated. Furthermore, it is recognized that even under clear-sky conditions, water vapor will affect the accuracy of the IST calculation. There is likely to be more water vapor in the boundary layer when melt ponds and leads are present, but this is handled by the algorithm automatically. The coefficients are primarily used to correct for atmospheric water vapor.

The primary difficulty with surface temperature retrieval occurs when melt ponds and leads are present. The emissivity over water will be somewhat lower than that of snow or ice, say 0.96 compared to 0.99. This will make a difference of a few tenths of a degree (J. Key, written communication, 1996). The directional effects are also probably slightly different in melt ponds and leads as compared to snow- or ice-covered sea ice.

4.5.5 Sources of Error

Sea ice identification does not have many of the complicating factors of varying surface covers that affect snow mapping, but there are complications that make sea ice mapping difficult. Because sea ice can vary in concentration from near zero to 100 percent, sea ice can give different reflectances and surface

temperatures even within a scene, due to mixed-pixel effects. Sea ice can also have different reflectances depending on snow cover and the presence of surface melt ponds. The presence of melt ponds and leads in the summer months will also affect the emissivity of the ice surface and therefore the calculation of ice surface temperature.

The accuracy of the IST is in the range of 0.3 - 2.1° K (Key *et al.*, 1997). An expected accuracy for the MODIS IST product will be based on accuracies reported in Key and Haefliger (1992), Lindsay and Rothrock (1994) and Key *et al.* (1997), and on investigation with MODIS Airborne Simulator data, which should allow us to define the expected accuracy for the MODIS IST.

Initially the coefficients of Key *et al.* (1997) can be used in the MODIS IST algorithm. The coefficients may be modified based on validation studies, or by inclusion of a quantitative method to correct for atmospheric effects based on modeling of the atmosphere or quantitative measurements of water vapor from another sensor, or based on an Arctic climatology database.

Another method for customizing the coefficients to the MODIS sensor is to model snow covered ice emissivity, MODIS sensor response, and the atmosphere to determine the estimated difference between the theoretical surface temperature, radiance measured by the sensor and the IST resulting from Equation [4]. The coefficients could be modified to allow agreement between the modeled and measured IST temperatures. Such methodology would follow the methods used by Key and Haefliger (1992) and Key *et al.* (1997).

MODIS Airborne Simulator (MAS) data are currently used to prototype the MODIS IST. Use of MAS data and associated field campaign data will be used to establish bounds for accuracy of MODIS IST, modification of coefficients, and other parameterizations of the algorithm and product generated.

Clouds pose many of the same problems in mapping sea ice as they do when mapping snow. Sea ice may move relatively rapidly and clouds may obscure this movement or make the movement of the sea ice appear incoherent when a 8-day time series, partially obscured by clouds, is compiled. Small ice floes, polynyas, and leads at subpixel resolution contribute error to identification and mapping of sea ice. Global error analysis will be accomplished with other sources of data, e.g. passive-microwave and regional operational sea ice data products, to estimate error at regional and global scales in the post-launch time period.

4.6 Gridding of Snow cover and Sea Ice Cover Data Products

The snow and sea ice data products will be generated and gridded to a common grid. The snow and lake ice maps will be gridded in a sinusoidal projection

common to the MODIS land group, at 500-m resolution. The sea ice maps will be re-gridded to a polar-stereographic map projection at 1-km resolution.

5.0 VALIDATION

5.1 Pre-Launch Validation Activities

5.1.1 Snow cover

5.1.1.1 Comparison with Sierra Nevada Snow Map derived from the 10 May 1992 TM Scene

Absolute accuracy can only be determined when Snowmap results are compared to ground measurements, or air photos that have been validated by field measurements. The snow covered area from Snowmap is compared with a TM scene of the Sierra Nevada Mountains, California, acquired on 10 May 1992 and mapped using an independently-produced snow-mapping algorithm called Snow covered Area (SCA) (Rosenthal, 1993; Rosenthal and Dozier, 1996). SCA is based on spectral-mixture modeling. A "learning sample" of several thousand pixels is selected in order to create a decision-tree algorithm that will eventually classify the scene. The final decision tree algorithm is optimized, representing a balance between speed (simplicity) and accuracy in identifying snow. The SCA algorithm has been verified with low-altitude, high-resolution aerial photography and ground-based measurements, thus it provides a good test for Snowmap.

Visual inspection shows that Snowmap classifies a similar number of pixels as snow compared with SCA. Statistical comparison of Snowmap with the SCA algorithm for a 10 May 1992 Landsat Thematic Mapper (TM) scene in the Sierra Nevada Mountains, California, shows that Snowmap performs well as a binary snow indicator. 89% of pixels with 50% or greater snow cover according to the SCA algorithm, are classified by Snowmap as completely snow covered, and 79% of those with less than 50% snow cover are classified as snow-free by Snowmap. It should be noted that the performance of both the SCA and Snowmap algorithms varies depending on the Landsat scene used in the analysis (J. Shi, personal communication, 1997).

5.1.1.2 BOREAS Experiment/February 1994

During February of 1994, in connection with the BOREAS project, the MODIS Airborne Simulator (MAS) was flown on the ER-2 aircraft over Prince Albert National Park, Saskatchewan, Canada. Simultaneous field measurements and lower-level aircraft flights were also acquired. Snowmap was run on five Landsat TM scenes (Table 2). Analysis of Northern Hemisphere weekly snow cover charts and field observations suggested that snow cover was approximately

100% for 1/18/93, 2/6/94, and 3/29/95 and approximately 0% for 8/6/90 and 9/21/95. For the 3 winter scenes, Snowmap mapped 99.9%, 85.7%, and 94.9% respectively of the Landsat scene as snow covered. For the two summer scenes the algorithm mapped 0.01% and 0.03% of the scene as snow covered (Klein *et al.*, in press). This indicates that the Snowmap algorithm is performing very well at mapping snow in this forested area.

Comparison of Snowmap with an older version of the algorithm without the NDVI correction showed that Snowmap mapped up to 37.3% more snow under some tree canopies. The NDSI-NDVI enhancement was particularly effective at improving the amount of snow mapped under dense older growth trees. Minimal differences were found between the two algorithms for snow cover over frozen lakes and in disturbed areas.

5.1.1.3 Upper Rhein-Felsburg Basin, Swiss Alps Study, 1994

A comparison of Snowmap with the Swiss Institute of Technology (ETHZ) snow-mapping algorithm was performed for a portion of two Landsat TM scenes (5/25/94 and 7/12/94) covering the upper Rhein-Felsburg basin. The areal extent of snow in this basin has been periodically mapped using Landsat TM, MSS and SPOT-XS images (Seidel *et al.*, 1997). The snow-mapping technique employed is more sophisticated than the MODIS snow-mapping algorithm. A Digital Elevation Model (DEM) is utilized to segment the satellite images into different illumination classes prior to classifying bare ice, snow covered, snow-free, and transition zones (50% snow covered) using multivariate statistics (Ehrler and Seidel, 1995).

For the 5/25/94 scene, Snowmap mapped 84.7% of the snow covered zone as snow, 47.9% of the transitional zone as snow, and 4.4% of the snow-free zone as snow. This shows that Snowmap performs well in this area when compared with a much more detailed site-specific snow model. For the 7/12/94 scene, Snowmap performed less well. The algorithm mapped 54.1%, 21.3%, and 1.5% of the snow covered, transitional, and snow-free zones as snow. It is unclear why these large errors of omission are present, however it is hypothesized that snow aging and metamorphosis may be responsible. Further investigation incorporating several other scenes is required and will be done after launch of the MODIS instrument.

5.1.1.4 April 1995 Alaska Experiment

In April 1995, the MODIS Airborne Simulator (MAS) on-board the ER-2 aircraft was deployed to image snow cover in Alaska and sea ice in the Bering Sea in conjunction with snow ground truth data collection. Also on-board was the Millimeter Wave Imaging Radiometer (MIR) instrument, which acquires images in

the microwave part of the spectrum. U.S. Army Cold Regions Research and Engineering (CRREL) and University of Alaska (Matthew Sturm and Carl Benson, respectively) scientists collaborated on analysis of the field and aircraft measurements.

An objective of the mission was to determine the accuracy of mapping snow in different surface covers. The surface cover in this area of central Alaska is typically spruce, birch, aspen, mixed forest, and muskeg. A vegetation density map was constructed using MAS data acquired on 4/13/95 (Hall *et al.*, in press). In regions having a vegetation-cover density of < 50%, Snowmap mapped 99% snow cover. These areas are generally composed of muskeg and mixed forests including frozen lakes. In the part of the scene that was estimated to have a vegetation-cover density ≥ 50%, Snowmap mapped 98% snow cover. These areas are generally composed of dense coniferous or deciduous forests. Without the NDVI component included in the Snowmap algorithm, only 71% of the snow cover was mapped in the forests. It can be seen that the revised algorithm clearly performs better in high density vegetation-cover.

5.1.1.5 New England/Wisconsin Mission, January and February 1997

During the Northern Hemisphere snow season, daily snow cover maps are created for the conterminous United States by the National Operational Hydrologic Remote Sensing Center (NOHRSC). Unlike the fully-automated process that is used to produce Snowmap products, NOHRSC products utilize the talents of highly-trained operators with considerable experience in mapping snow in North America. In the post-launch period NOHRSC products will be a primary dataset for comparison with MODIS snow cover products.

Snow cover for a Landsat TM scene (2/13/97) derived from Snowmap and the NOHRSC algorithm were compared. This scene covers an area in southern New York and portions of Pennsylvania, New Jersey, and Connecticut. Extensive snow covered areas were present in the image and large tracts of both images are forested. Field work conducted on 2/9/97, as part of the 1997 WINter Cloud Experiment (WINCE), indicated that snow cover was extensive in both forested and non-forested areas at the time of image acquisition. Given the different resolutions of the inputs into the NOHRSC and Snowmap algorithms, only qualitative comparisons are possible. It can be seen from Figure 6, however, that there is a very good correspondence between the snow covered area derived from the two methods. Also shown is the substantial improvement of the enhanced Snowmap algorithm over the original.

5.1.2 Snow Albedo

*** Section to be included in the near future ***

5.1.3 Sea Ice

The Icemap algorithm has been tested using a MAS scene over the Bering Sea near St. Lawrence Island, Alaska, acquired on 8 April 1995. Sea ice extent was mapped using a combination method based on the surface reflectance in the visible and near-infrared and the ice surface temperature (Riggs et al., in press). From the combination method, snow covered sea ice and snow-free thin ice could also be determined. Although no ground-based data were collected, the ice extent and ice type maps derived from the MAS scene were in general agreement with visual interpretation of sea ice in the scene. Furthermore, the results agreed well with previous studies performed in the same region (e.g. Massom and Comiso, 1994).

5.2 Post-Launch Validation Activities

5.2.1 Snow Cover

Focused field campaigns will be set up to do post-launch validation. The first post-launch field and aircraft mission will be requested for February of 1999. Snow cover will be measured using field measurements and MAS underflights in the eastern and mid-western United States. Flights will be flown in various land covers: agricultural, alpine, forest and prairie. Field and low-level, high-resolution aircraft measurements will also be acquired. Snowmap-derived errors in snow mapping in each of these categories will be re-examined.

5.2.1.1 Comparison with Other Global-Scale Products

Snowmap results will be compared with other snow cover maps and existing data sets of snow cover to determine relative error. The NOAA weekly snow charts and the NOHRSC regional data sets are good for comparison with Snowmap results generated from MODIS. The data sets have an historical record and are generated operationally. Snowmap results will also be compared with snow cover derived from Scanning Multichannel Microwave Imager (SSM/I) data, if available, or Advanced Microwave Scanning Radiometer (AMSR) data after the launch of the first EOS-PM platform in 2000. Comparison of Snowmap results with these independently-produced snow data sets will allow errors to be identified that will permit us to determine the accuracy of the global maps relative to one another.

NOAA has recently launched the NOAA-K satellite which has an AVHRR instrument enhanced with a 1.6 μm channel for snow and cloud discrimination. The 1.6 μm channel on NOAA-K will be available for testing in February of 1999, but not for regular use. A change in the technique for the generation of NOAA snow and ice charts is expected with the launch of NOAA-L. At that time, a

snow/cloud discrimination technique using the 1.6 μm channel will probably be implemented. The techniques used by NOAA and the snow and ice data sets they generate can then be used for validation for MODIS snow and cloud discrimination techniques employing the MODIS 1.6 μm band. NOAA experience for snow/cloud discrimination with satellite data at 1.6 μm will be drawn upon for refinement of Snowmap in the near-launch time frame. We are working closely with the NOAA/NESDIS group so we can share ideas and algorithms for snow cover mapping and validation.

5.2.2 Sea Ice

Algorithm development and analysis will continue with current and future MAS and MODIS data. The Icemap algorithm can be easily adapted should these validation studies show specific regional or seasonal differences. Comparisons of sea ice extent and ice type with products derived from passive and active microwave data are planned for the post-launch period.

6.0 COMBINATION OF MODIS AND OTHER EOS DATA

The combined use of visible, near-IR, short-wave IR and microwave sensors to map snow will lead to an ability to map snow extent, albedo, water equivalent, and sea ice concentration. Because passive-microwave sensors are generally unaffected by cloud-cover over snow- and ice-covered areas, it will be advantageous, in the EOS era after the launch of the second EOS platform, to use MODIS data in conjunction with Advanced Microwave Scanning Radiometer (AMSR) data to map snow extent and depth globally. Algorithms are currently being developed which combine AVHRR and SSM/I data, to more accurately map snow cover. These algorithms will be modified to use MODIS and AMSR data when these data become available. Also, the Advanced Microwave Sounding Units (AMSU-A and AMSU-B) aboard the NOAA-K satellite will be used for validation. Many of our pre-launch validation efforts deal with combining the optical and passive-microwave data. For example, the Alaska 1995 and WINCE 1997 missions had the Millimeter-wave Imaging Radiometer (MIR) as well as the MAS on board (Hall *et al*., 1996, Tait *et al*., in press (a) and (b)).

Passive-microwave data have been used to map Northern Hemisphere snow cover at a resolution of up to 30 km since 1978 even through darkness and cloud-cover. The passive-microwave data also provide an estimate of snow-water equivalent in many areas. Parameters affecting the passive-microwave response of snow include: water equivalent, density, grain size, temperature, surface roughness, forest-cover fraction and forest type. Problems inherent in the interpretation of the data include: the coarse resolution is not suitable for most regional snow studies, in densely-forested areas algorithms underestimate

snow-water equivalent, and derivation of snow-water equivalent is dependent upon snow and land-cover characteristics.

Similarly, passive-microwave data have been used to map sea ice extent and concentration. In the future, with AVHRR data from NOAA-K and beyond, and with MODIS data, optical data can be used to provide detail that passive-microwave data cannot, including IST, when conditions are clear. Used in synergy, optimum sea ice information will be possible.

6.1 Analysis of Snow cover in Alaska using Aircraft Microwave Data, 1995

From 31 March to 25 April, 1995, a mission was conducted to study snow cover in northern and central Alaska, respectively (Hall *et al.*, 1996; Tait *et al.*, in press (a)). The utility of high frequency passive-microwave aircraft data was examined, as was the influence of a variety of surface cover types on the microwave brightness temperatures of dry and melting snow. The aircraft data included the Millimeter-wave Imaging Radiometer (MIR) and the MODIS Airborne Simulator (MAS).

The MIR is a mechanically-scanned imaging microwave radiometer that measures radiation at the following frequencies: 89, 150, 183.3±1, 183.3±3, 183.3±7 and 220 GHz. It has an angular resolution of about 3.5°. It is a cross-track scanner with an angular swath width of about 100°, centered at nadir. Its polarization vector is in the horizontal plane and perpendicular to the velocity vector of the aircraft so that the measured radiation is a mixture of vertical and horizontal polarizations depending on the viewing angles. The temperature sensitivity is ≤ 1 K for all channels. The MIR data in this study have a spatial resolution of approximately 1 km at nadir.

Field measurements of snow depth, density, grain size and shape were made in Fairbanks (64°50'N, 147°48'W) and at Ester Dome which is about 5 km northwest of Fairbanks, as well as in other parts of Alaska. Aircraft flight lines were flown in a grid pattern in central Alaska, including Fairbanks, on 5, 6, 13 and 21 April. The MAS data were scaled to the MIR resolution, and vegetation data (Kuchler, 1985), were also re-projected.

Field and air-temperature measurements showed that the snow in and near Fairbanks was melting during the daytime during the month of April. Except within the city, snow cover was nearly continuous. Table 3 shows snow depths from a location in Fairbanks and at Ester Dome. Table 4 shows air temperatures at the approximate time of the aircraft takeoff on the flight days over the 'Fairbanks grid.' Each flight over the Fairbanks grid lasted about 2 hours and 20 minutes.

Snow in Fairbanks was actively melting during the daytime during the month of April. As soon as snow becomes wet, scattering is reduced as the crystals become coated with liquid water. As a result, the snowpack behaves as a lossy medium, and the brightness temperature increases. In the vicinity of Fairbanks, the 89 GHz brightness temperatures (T_Bs) averaged 263 K, while in the southern part of the study area (central Alaska Range) T_Bs were ≅210 K on 5 April. Deeper snow and lower temperatures contributed to lower T_Bs there. Additionally, on lines flown north of Fairbanks, toward the Brooks Range and on the North Slope, also on 5 April, T_Bs are 10-40 K lower than in the Fairbanks area because the snow to the north was still dry in April. Also, in the Brooks Range and on the North Slope, there are no trees to increase the T_Bs there.

Comparison of the vegetation map with the MIR data shows that several land-cover types influence the microwave signal. On each of the 4 MIR images (at 89 GHz) for the Fairbanks grid, a boundary between the black spruce forest and the meadow dryas is evident at a latitude of approximately 64°N, just south of Fairbanks. Coniferous trees emit more microwave radiation than do tundra or dryas vegetation, and this is one explanation for the higher T_Bs in the black spruce forests.

In the central part of the Fairbanks grid, T_Bs are generally quite high due to the melting snow. The relatively high T_Bs there overwhelm the brightness-temperature differences that result from land-cover variability. This is especially true on April 13, when the air temperatures were the highest of the 4 flight days (Table 4), and presumably, when melting covered the largest extent of area.

Other regions of interest are where finger-like projections of the spruce-birch forest to the east of Fairbanks intersect dryas meadows and barren areas. T_Bs are higher in the spruce-birch forest (≅261 K) than in the dryas meadows and barren areas (≅251 K) presumably due to the higher emissivity of the trees.

Table 4. Snow depths in Fairbanks and at Ester Dome on selected dates in April.

Date	Fairbanks	Ester Dome
4/1/95	59 cm	---
4/2/95	54 cm	---
4/6/95	39 cm	---
4/7/95	35 cm	---
4/8/95	---	100 cm
4/11/95	23 cm	---

Table 5. Average air temperatures at approximate times of aircraft takeoffs, and time of flights over the 'Fairbanks grid.'

Date	°C	Fairbanks local time
4/5/95	8°	10:50 - 13:11
4/6/95	3°	8:42 - 11:01
4/13/95	10°	11:08 - 13:36
4/21/95	-1°	6:59 - 9:29

The land-cover type is shown to influence microwave brightness temperature under dry snow conditions. Snow covered forests cause higher T_Bs than do snow covered dryas meadows and tundra. However, when the snowpack is wet, the high emissivity of the snowpack overwhelms the contribution of the vegetation to the brightness temperature.

Work will continue on the current data set to investigate the influence of land cover, particularly the influence of the dryas meadows and black spruce. Satellite data will be analyzed in conjunction with MIR data in order to modify snow depth retrieval algorithms so that they are more responsive to the snow and land surface conditions encountered in central and northern Alaska. In addition, analysis of MIR and MAS data, together, will be undertaken.

6.2 Analysis of Snow cover in the Northeastern United States using Aircraft Microwave Data, 1997

The MIR and MAS instruments were flown onboard the NASA ER-2 aircraft as part of the WINter Cloud Experiment (WINCE) in January and February 1997. Comparison of the snow covered area derived from Snowmap (using MAS channels 2 and 10) and the 89 GHz brightness temperature data for several different land covers indicated a strong relationship (Tait *et al.*, in press (b)). In snow-free areas the mean T_B is 265 K compared with 180 K in snow covered areas. Furthermore, the 89 GHz data were able to effectively detect snow even under clouds, when the MAS instrument was unable to view the surface. It is suggested that T_B data may be extremely beneficial for mapping snow in cloudy conditions, as a supplement to the Snowmap output.

Although the results of the WINCE snow-mapping experiment using the 89 GHz data are very encouraging, it should be noted that they could not be replicated over Alaska using the 1995 data. It is hypothesized that the presence of liquid water within the snowpack and in the soil disturbed the snow-brightness

temperature relationship to the extent that the model was unusable. In addition, while the MIR data were almost completely impervious to clouds during the WINCE mission, this was not the case over Alaska. Here, clouds had a significant impact on the high-frequency microwave data. This may be due to warmer air temperatures and hence a greater moisture-holding capacity of air masses during the Alaska mission compared with the WINCE mission. A full analysis of the potential of 89 GHz data in conjunction with Snowmap is proposed during the post-launch time period. Data from AMSU-A and AMSU-B will be compared with the MODIS output.

7.0 References

Assel, R.A., T.E. Croley II and K. Schneider, 1994: Normal daily temperatures and ice cover of the Laurentian Great Lakes of North America, Abstract only, 51st Eastern Snow Conference, 15-16 June 1994, Dearborn, MI.

Barry, R.G., 1986: The sea ice data base, In: The Geophysics of Sea Ice, Untersteiner, N. (ed.), Plenum Press, NY, pp 1099-1134.

Bromwich, D.H., R.-Y. Tzeng and T.R. Parish, 1994: Simulation of the modern arctic climate by the NCAR CCM1, Journal of Climate, 7, pp 1050-1069.

Bunting, J.T. and R.P. d'Entremont, 1982: Improved cloud detection utilizing defense meteorological satellite program near infrared measurements, Air Force Geophysics Laboratory, Hanscom AFB, MA, AFGL-TR-82-0027, Environmental Research Papers, No. 765, 91 p.

Carsey, F.D., 1992: Microwave Remote Sensing of Sea Ice, American Geophysical Union, Geophysical Monograph 68, 462 p.

Carroll, T.R., 1990: Operational airborne and satellite snow cover products of the National Operational Hydrologic Remote Sensing Center, Proceedings of the forty-seventh annual Eastern Snow Conference, June 7-8, 1990, Bangor, Maine, CRREL Special Report 90-44.

Chang, A.T.C., J.L. Foster and D.K. Hall, 1987: Microwave snow signatures (1.5 mm to 3 cm) over Alaska, Cold Regions Science and Technology, 13, pp 153-160.

Chapman, W.L. and J.E. Walsh, 1993: Recent variations of sea ice and air temperature in high latitudes, Bulletin of the American Meteorological Society, 74, pp 33-47.

Choudhury, B.J. and A.T.C. Chang, 1981: The albedo of snow for partially cloudy skies, Boundary Layer Meteorology, 20, pp 371-389.

Clarke, A.D. and K.J. Noone, 1985: Soot in the Arctic snowpack: a cause for perturbations in radiative transfer. Atmospheric Environment, 19, pp 2045-2053.

Comiso, J.C., 1994: Surface temperatures in the polar regions from Nimbus-7 temperature humidity infrared radiometer. Journal of Geophysical Research, 99(C3), pp 5181-5200.

Comiso, J.C., P. Wadhams, W.B. Drabill, R.N. Swift, J.P. Crawford and W.B. Tucker III, 1991: Top/bottom multisensor remote sensing of arctic sea ice. Journal of Geophysical Research, 96(C2), pp 2693-2709.

Conway, H., A. Gades and C.F. Raymond, 1996: Albedo of dirty snow during conditions of melt, Water Resources Research, 32, pp 1713-1718.

Dirmhirn, I. and F.D. Eaton, 1975: Some characteristics of the albedo of snow. Journal of Applied Meteorology, 14, pp 375-379.

Dozier, J., S.R. Schneider and D.F. McGinnis Jr., 1981: Effect of grain size and snowpack water equivalence on visible and near-infrared satellite observations of snow. Water Resources Research, 17, pp 1213-1221.

Dozier, J., 1984: Snow reflectance from Landsat-4 thematic mapper. I.E.E.E. Transactions on Geoscience and Remote Sensing, 22, pp 323-328.

Dozier, J., 1989: Spectral signature of alpine snow cover from the Landsat Thematic Mapper, Remote Sensing of Environment 28, pp 9-22.

Ehrler, C. and K. Seidel, 1995: Mutual effects of the climate change and the alpine snow cover and their influence on the runoff regime evaluated with the aid of satellite remote sensing. Proceedings of the IGARSS '95 Symposium, 1995, Florence, Italy, pp 1973-1975.

Foster, J.L., D.K. Hall, A.T.C. Chang and A. Rango, 1984: An overview of passive microwave snow research and results, Reviews of Geophysics, 22, pp 195-208.

Foster, J.L., A.T.C. Chang, D.K. Hall and A. Rango, 1991: Derivation of snow water equivalent in boreal forests using microwave radiometry, Arctic, 44 (Supp. 1), pp 147-152.

Gao, B.-C., A.F.H. Goetz and W.J. Wiscombe, 1993: Cirrus cloud detection from airborne imaging spectrometer data using the 1.38 mm water vapor band, Geophysical Research Letters, 20(4), pp 301-304.

Grenfell, T.C. and D.K. Perovich, 1984: Spectral albedos of sea ice and incident solar irradiance in the southern Beaufort Sea, Journal of Geophysical Research, 89(C3), pp 3573-3580.

Hall, D.K., J.L. Foster and A.T.C. Chang, 1982: Measurement and modeling of microwave emission from forested snowfields in Michigan, Nordic Hydrology, 13, pp 129-138.

Hall, D.K., A.T.C. Chang, J.L. Foster, C.S. Benson and W.M. Kovalick, 1989: Comparison of in-situ and Landsat-derived reflectance of Alaskan glaciers, Remote Sensing of Environment, 28, pp 23-31.

Hall, D.K. (ed.), 1995: Proceedings of the First MODIS Snow and Ice Workshop, 15-17 September 1995, Greenbelt, MD, 128 p.

Hall, D.K., G.A. Riggs and V.V. Salomonson, 1995: Development of methods for mapping global snow cover using moderate resolution imaging spectroradiometer data, Remote Sensing of Environment, 54, pp 127-140.

Hall, D.K., J.L. Foster, A.T.C. Chang, D.J. Cavalieri and J.R. Wang, 1996: Analysis of snow cover in Alaska using aircraft microwave data (April 1995), Proceedings of the IGARSS '96 Symposium, 27-31 May 1996, Lincoln, NE, 4, pp 2246-2248.

Hall, D.K., J.L. Foster, V.V. Salomonson, A.G. Klein and J.Y.L. Chein, 1998: Error analysis for global snow cover mapping in the Earth Observation System (EOS) Era, CD-ROM Proceedings of the IGARSS '98 Symposium, 7-13 July 1998, Seattle, WA.

Hall, D.K., J.L. Foster, A.T.C. Chang, C.S. Benson and J.Y.L. Chein, in press: Determination of snow covered area in different land covers in central Alaska, U.S.A., from aircraft data - April 1995, submitted to Annals of Glaciology, 26, 1998.

Key, J.R. and M. Haefliger, 1992: Arctic ice surface temperature retrieval from AVHRR thermal channels, Journal of Geophysical Research, 97(D5), pp 5885-5893.

Key, J.R., J.A. Maslanik, T. Papakyriakou, M.C. Serreze and A.J. Schweiger, 1994. On the validation of satellite-derived sea ice surface temperature, Arctic, 47, pp 280-287.

Key, J.R., J.B. Collins, C. Fowler and R.S. Stone, 1997: High-latitude surface temperature estimates from thermal satellite data, Remote Sensing of Environment, 61, pp 302-309.

King, M.D., Y.K. Kaufman, W.P. Menzel and D. Tanre, 1992: Remote sensing of cloud, aerosol, and water vapor properties from the moderate resolution imaging spectrometer (MODIS), IEEE Transactions on Geoscience and Remote Sensing, 30, pp 2-27.

Klein, A.G., D.K. Hall and G.A. Riggs, 1998: Global snow cover monitoring using MODIS, Proceedings of the 27th International Symposium on Remote Sensing of Environment, Tromso, Norway, pp 830-833.

Klein, A.G., D.K. Hall and G.A. Riggs, in press: Improving snow cover mapping in forests through the use of a canopy reflectance model, submitted to Hydrological Processes.

Kuchler, A.W., 1985: Potential Natural Vegetation, USGS Map from National Atlas, sheet no. 89.

Kyle, H.L., R.J. Curran, W.L. Barnes and D. Escoe, 1978: A cloud physics radiometer, Third Conference on Atmospheric Radiation, Davis, CA, pp 107-109.

Lindsay, R.W. and D.A. Rothrock, 1993: The calculation of surface temperature and albedo or Arctic sea ice from AVHRR, Annals of Glaciology, 17, pp 391-397.

Lindsay, R.W. and D.A. Rothrock, 1994: Arctic sea ice temperature from AVHRR, Journal of Climate, 7, pp 174-183

Liston, G.E., 1995: Local advection of momentum, heat, and moisture during the melt of patchy snow covers. Journal of Applied Meteorology, 34(7), pp 1705-1715.

Markham, B.L. and J.L. Barker, 1986: Landsat MSS and TM post-calibration dynamic ranges, exoatmospheric reflectances and at-satellite temperatures, EOSAT Technical Notes, No. 1, August, pp 3-8.

Massom, R., and J.C. Comiso, 1994. The classification of Arctic sea ice types and the determination of surface temperature using advanced very high resolution radiometer data, Journal Geophysical Research, 99(C3), pp 5201-5218.

Matson, M., C.F. Ropelewski and M.S. Varnadore, 1986: An atlas of satellite-derived northern hemisphere snow cover frequency, National Weather Service, Washington, D.C., 75 pp.

Matson, M., 1991: NOAA satellite snow cover data, Palaeogeography and Palaeoecology, 90, pp 213-218.

O'Brien, H.W. and R.H. Munis, 1975: Red and near-infrared spectral reflectance of snow. In: Operational Applications of Satellite Snow cover Observations, edited by A. Rango, NASA SP-391 (Washington, D.C.: NASA), pp 345-360.

Palecki, M.A. and R.G. Barry, 1986: Freeze-up and break-up of lakes as an index of temperature changes during the transition seasons: a case study in Finland, Journal of Climate and Applied Meteorology, 25, pp 893-902.

Parkinson, C.L., J.C. Comiso, H.J. Zwally, D.J. Cavalieri, P. Gloersen and W.J. Campbell, 1987: Arctic Sea Ice, 1973-1976: Satellite Passive-Microwave Observations, NASA SP-489, GPO, Washington, D.C.

Rango, A., 1993: Snow hydrology processes and remote sensing, Hydrological Processes, 7, pp 121-138.

Rango, A. and J. Martinec, 1982: Snow accumulation derived from modified depletion curves of snow coverage, Symposium on Hydrological Aspects of Alpine and High Mountain Areas, IAHS Publication No. 138, pp 83-90.

Riggs, G.A., D.K. Hall and V.V. Salomonson, in press: Sea ice extent classification mapping with the Moderate Resolution Imaging Spectroradiometer Airborne Simulator, Remote Sensing of Environment.

Robinson, D.A., K.F. Dewey and R.R. Heim Jr., 1993: Global snow cover monitoring: an update. Bulletin of the American Meteorological Society, 74, pp 1689-1696.

Rosenthal, W., 1993: Mapping montane snow cover at subpixel resolution from the Landsat thematic mapper, Univ. of California Santa Barbara M.A. thesis, 70 p.

Rosenthal, W. and J. Dozier, 1996: Automated mapping of montane snow cover at subpixel resolution from the Landsat Thematic Mapper, Water Resources Research, 32, pp 115-130.

Rossow, W.B. and L.C. Garder, 1993: Validation of ISCCP cloud detection, Journal of Climate, 6(12), pp 2370-2393.

Salomonson, V.V. and D.C. Marlatt, 1968: Anisotropic solar reflectance over white sand, snow and stratus clouds. Journal of Applied Meteorology, 7, pp 475-483.

Salomonson, V.V. and D.L. Toll, 1991: The moderate resolution imaging spectrometer-radar (MODIS-N) facility instrument, Advances in Space Research, 11, pp 231-236.

Schindler, D.W., K.G. Beaty, E.J. Fee, D.R. Cruikshank, E.R. DeBruyn, D.L. Findlay, G.A. Linsey, J.A. Shearer, M.P. Stainton and M.A. Turner, 1990: Effects of climatic warming on lakes of the central boreal forest. Science, 250, pp 967-970.

Seidel, K., C. Ehrler and J. Martinec, 1997: Effects of climate change on water resources and runoff in an alpine basin, Proceedings of the 1997 Eastern Snow Conference, Banff, Alberta, May 4-8, pp 221-228.

Singer, F.S. and R.W. Popham, 1963: Non-meteorological observations from weather satellites, Astronautics and Aerospace Engineering, 1(3), pp 89-92.

Steffen, K., 1987, Bidirectional reflectance of snow. In B.E. Goodison, R.G. Barry, and J.Dozier, (editors): Large scale effects of seasonal snow cover. Proceedings of the IAHS Symposium held in Vancouver on 19-22 August 1987 (Vancouver, Canada: IAHS), pp 415-425.

Tait, A.B., D.K. Hall, J.L. Foster and A.T.C. Chang, in press (a): High frequency passive microwave radiometry over a snow covered surface in Alaska, Photogrammetric Engineering and Remote Sensing.

Tait, A.B., D.K. Hall, J.L. Foster, A.T.C. Chang and A.G. Klein, in press (b): Detection of snow and vegetation cover using millimeter-wave radiometer data, Remote Sensing of Environment.

Townshend, J.R.G. and C.J. Tucker, 1984: Objective assessment of Advanced Very High Resolution Radiometer data for land cover mapping, International Journal of Remote Sensing 5, pp 497-504.

Tucker, C.J., 1979: Red and photographic infrared linear combinations for monitoring vegetation, Remote Sensing of Environment, 8, pp 127-150.

Tucker, C.J., 1986: Maximum normalized difference vegetation index images for sub-Saharan Africa for 1983-1985, International Journal of Remote Sensing, 7, pp 1383-1384.

Warren, S.G., 1982: Optical properties of snow. Reviews of Geophysics and Space Physics, 20, pp 67-89.

Warren, S.G. and A.D. Clarke, 1985: Soot from Arctic haze: Radiation effects on the Arctic snowpack. Snowwatch, World Data Center A for Glaciology (snow and ice) Report GD-18, edited by G. Kukla, R.G. Barry, A. Hecht and D. Wiesnet, Boulder, Colorado.

Warren, S.G. and W.J. Wiscombe, 1980: A model for the spectral albedo of snow II: snow containing atmospheric aerosols, Journal of the Atmospheric Sciences, 37, pp 2734-2745.

Winther, J.G., 1992: Landsat thematic mapper (TM) derived reflectance from a mountainous watershed during the snow melt season, Nordic Hydrology, 23, pp 273-290.

Wiscombe, W.J. and S.G. Warren, 1980: A model for the spectral albedo of snow I : pure snow, Journal of the Atmospheric Sciences, 37, pp 2712-2733.

Yu, Y., A. Rothrock and R.W. Lindsay, 1995: Accuracy of sea ice temperature derived from the advanced very high resolution radiometer, Journal of Geophysical Research, 100(C3), pp 4525-4532.

Zwally, H.J., J.C. Comiso, C.L. Parkinson, W.J. Campbell, F.D. Carsey and P. Gloersen, 1983: Antarctic Sea Ice, 1973-1976: Satellite Passive-Microwave Observations, NASA, SP-459, 206 p, G.P.O., Wash., D.C.

8.0 Figure Captions

1. Sequence of MODIS snow cover algorithms and data products. Three MODIS products (green rectangles) are the starting data input. The Earth Science Data Types (ESDT, cyan rectangles) generated by each algorithm (light gray rectangles) are the input for the next level of algorithms.

2. Sequence of MODIS sea ice algorithms and data products. Three MODIS products (green rectangles) are the starting data input. The Earth Science Data Types (ESDT, cyan rectangles) generated by each algorithm (light gray rectangles) are the input for the next level of algorithms. There are two ESDT products for each algorithm; a daytime and a nighttime product.

3. Spherical albedo of snow and clouds. (After King et al., 1992; O'Brien and Munis, 1975).

4. Histogram of snow and forest samples, and forest samples from 14 March 1991 and 03 September 1990 TM images, respectively, of Glacier National Park, Montana region. Snow sample from snow covered surface of frozen Lake McDonald (n=2025) from the 14 March 1991 scene. Snowy forest (n=1375) sample from a snow covered forest valley on the 14 March 1991 scene. Forest summer (n=2025) and winter (n=2025) samples from the same location in dense forest to the immediate west of Lake McDonald.

5. Major classification criteria used in the Snowmap algorithm. Pixels with an NDSI of greater than 0.4 are considered snow covered (hatched field). In addition, pixels with slightly lower NDSI, but high NDVI values are considered snow covered forests (gray polygon).

6. Snow cover maps from the (a) NOHRSC, (b) original MODIS and (c) enhanced MODIS (Snowmap) snow-mapping algorithms.

9.0 Appendix A

Product Level Descriptions

Level 0 - Raw instrument data at original resolution, time ordered, with duplicate packets removed.

Level 1A - Reconstructed unprocessed instrument data at full resolution, time referenced, and annotated with ancillary information, including radiometric and geometric calibration coefficients and georeferencing parameters (i.e. platform ephemeris) computed and appended, but not applied to Level 0 data.

Level 1B - Radiometrically-corrected and geolocated Level 1A data that have been processed to sensor units.

Level 2 - Derived geophysical parameters at the same resolution and location as the Level 1 data.

Level 2G - Level 2 geophysical parameters that have been gridded onto a specified Earth grid.

Level 3 - Geophysical parameters that have been spatially and/or temporally re-sampled (i.e., derived from Level 1 or Level 2 data).

Level 4 - Model output and/or results of lower-level data that are not directly derived by the instruments.

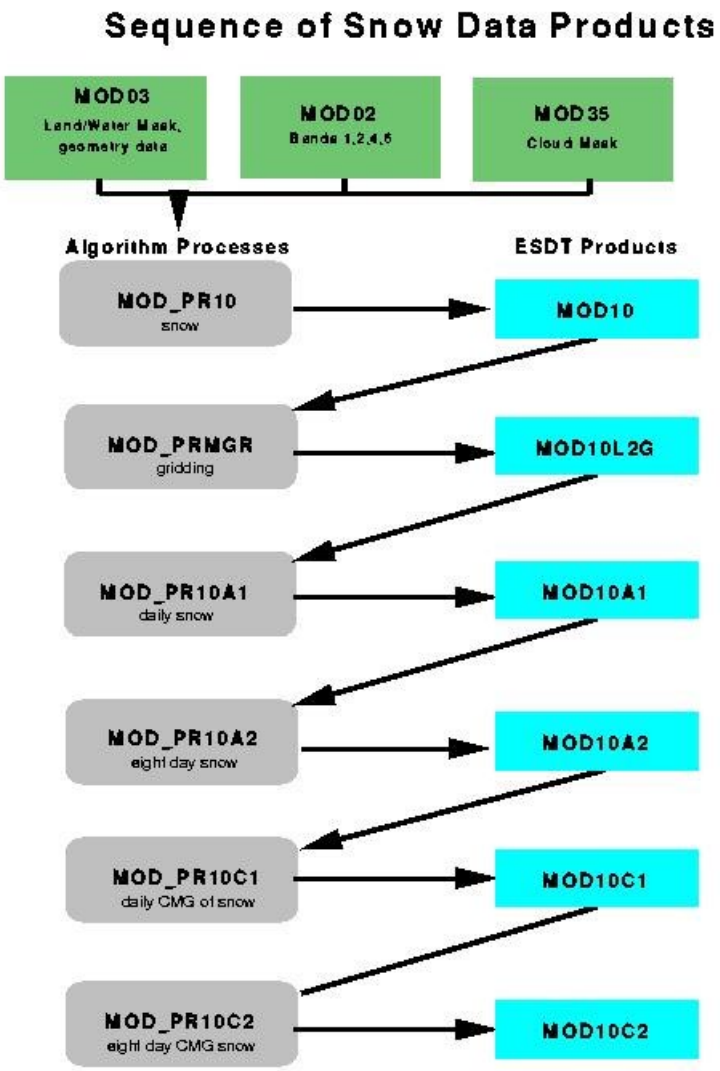
Sequence of Snow Data Products
MOD03
Land/Water Mask, geometry data
MOD02
Bands 1,2,4,6
MOD35
Cloud Mask
Algorithm Processes
ESDT Products
MOD_PR10
snow
MOD10
MOD_PRMGR
gridding
MOD10L2G
MOD_PR10A1
daily snow
MOD10A1
MOD_PR10A2
eight day snow
MOD10A2
MOD_PR10C1
daily CMG of snow
MOD10C1
MOD_PR10C2
eight day CMG snow
MOD10C2

Figure 1

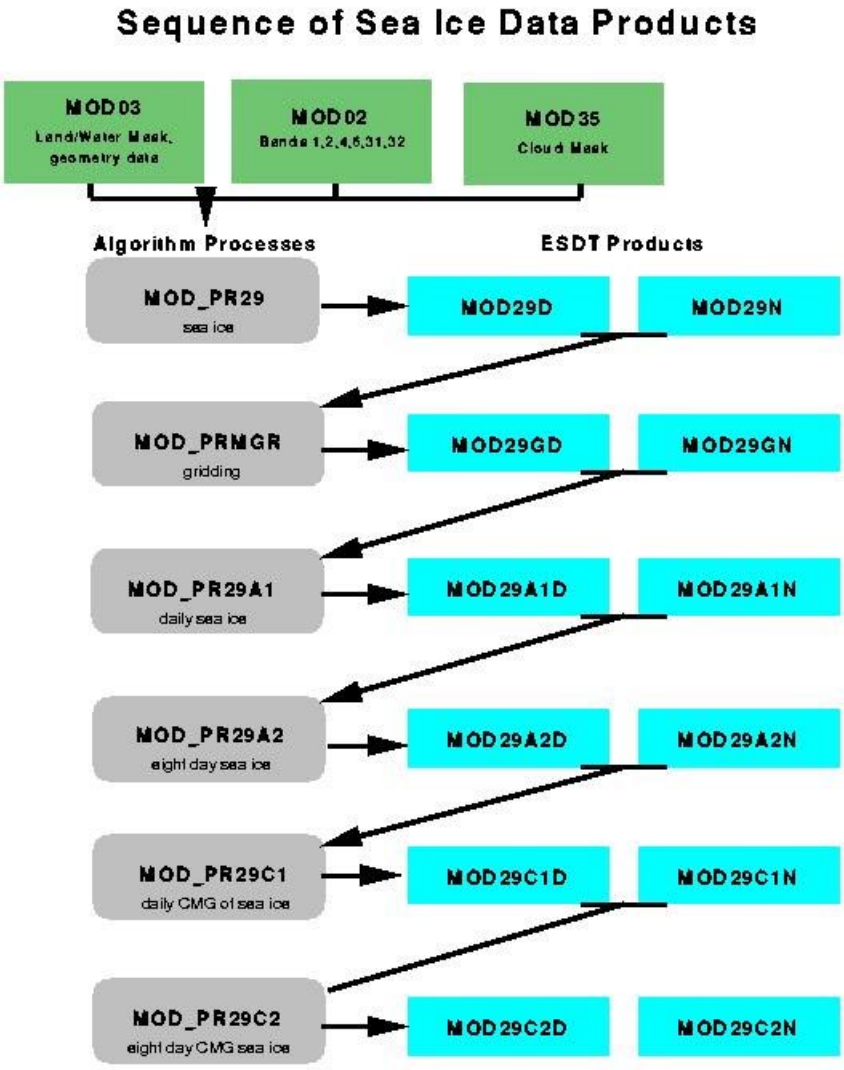
Sequence of Sea Ice Data Products
MOD03
Land/Water Mask, geometry data
MOD02
Bands 1,2,4,6,31,32
MOD35
Cloud Mask
Algorithm Processes
ESDT Products
MOD_PR29
sea ice
MOD29D
MOD29N
MOD_PRMGR
gridding
MOD29GD
MOD29GN
MOD_PR29A1
daily sea ice
MOD29A1D
MOD29A1N
MOD_PR29A2
eight day sea ice
MOD29A2D
MOD29A2N
MOD_PR29C1
daily CMG of sea ice
MOD29C1D
MOD29C1N
MOD_PR29C2
eight day CMG sea ice
MOD29C2D
MOD29C2N

Figure 2

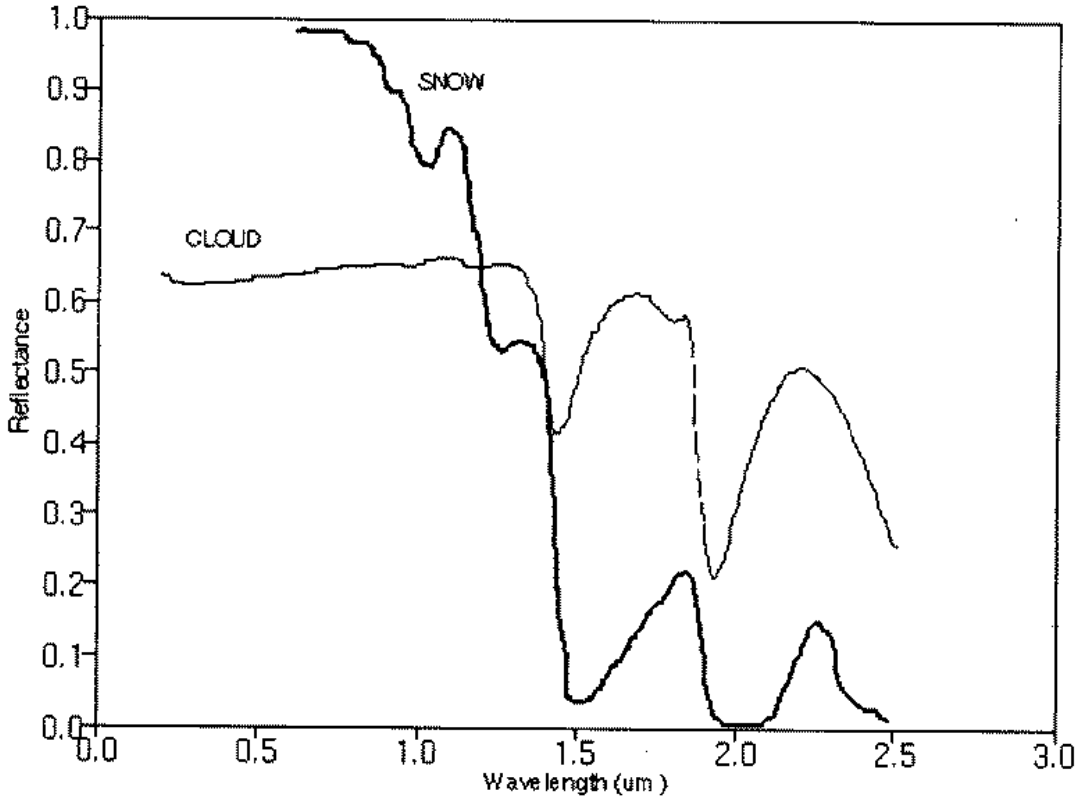
SNOW
CLOUD
Reflectance
Wavelength (um)
1.0
0.9
0.8
0.7
0.6
0.5
0.4
0.3
0.2
0.1
0.0
0.0
0.5
1.0
1.5
2.0
2.5
3.0

Figure 3

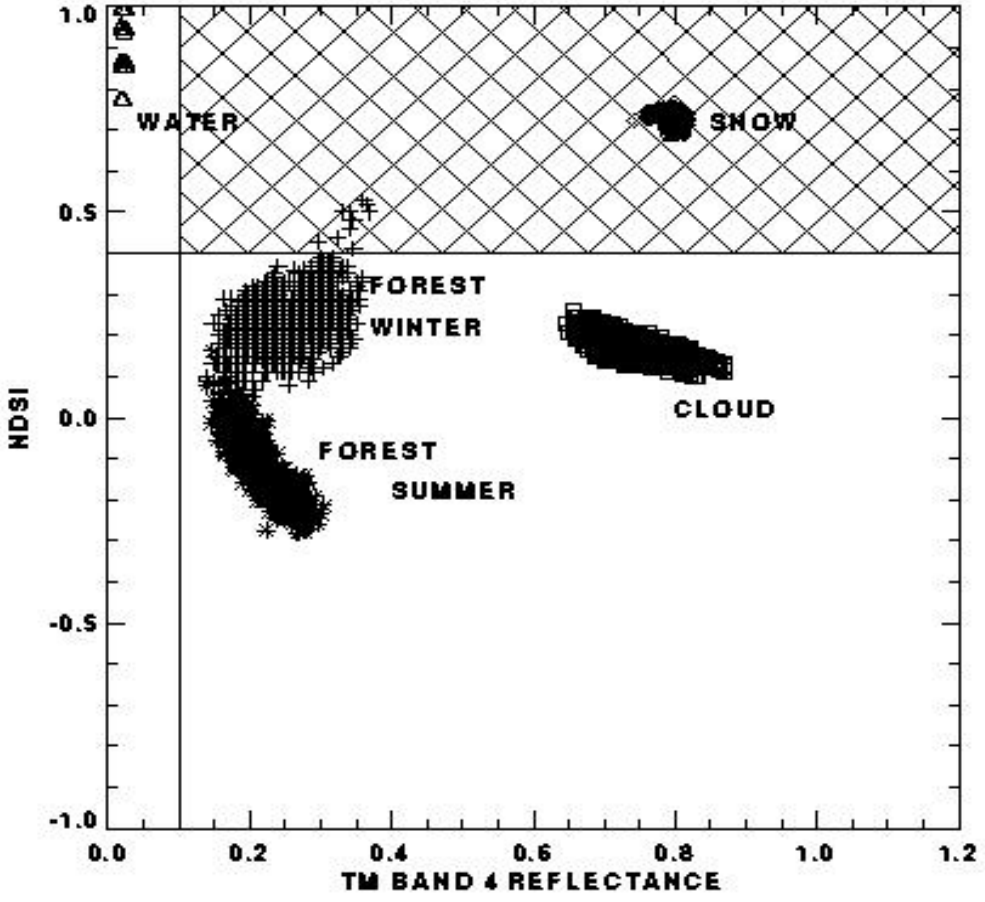
1.0
0.5
0.0
-0.5
-1.0
NDSI
0.0
0.2
0.4
0.6
0.8
1.0
1.2
TM BAND 4 REFLECTANCE
WATER
SNOW
FOREST
WINTER
CLOUD
FOREST
SUMMER

Figure 4

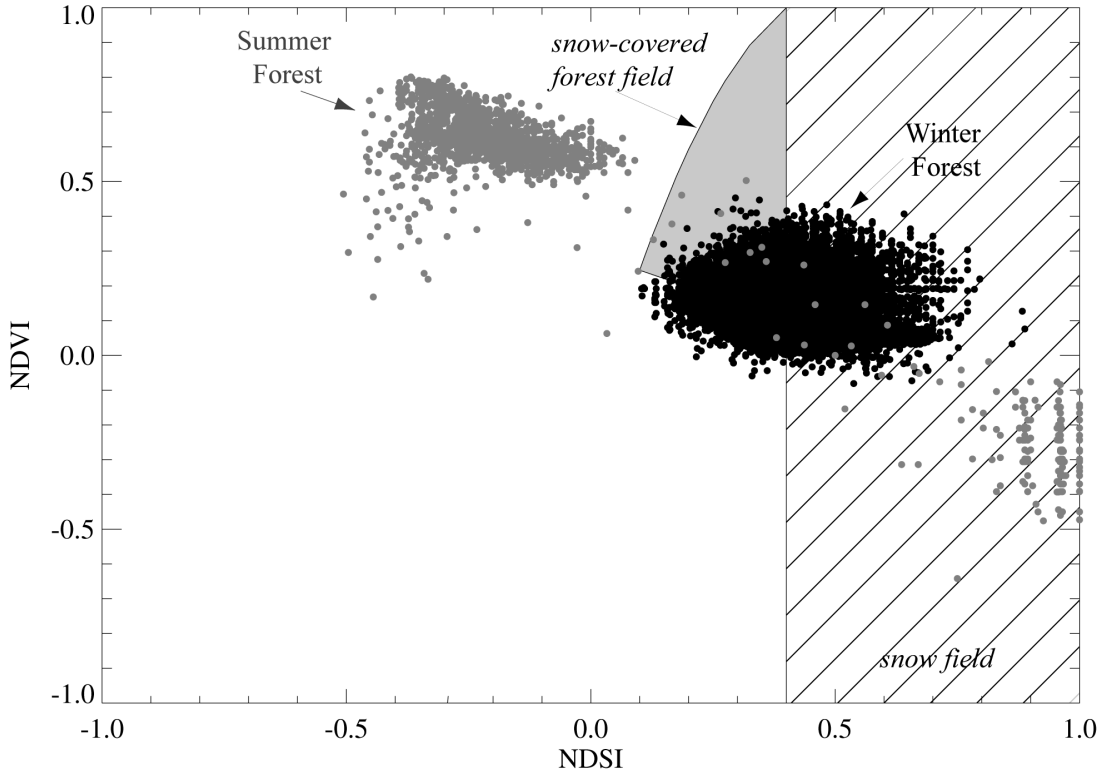
Summer
Forest
snow-covered
forest field
Winter
Forest
snow field
NDVI
NDSI
1.0
0.5
0.0
-0.5
-1.0
-1.0
-0.5
0.0
0.5
1.0

Figure 5

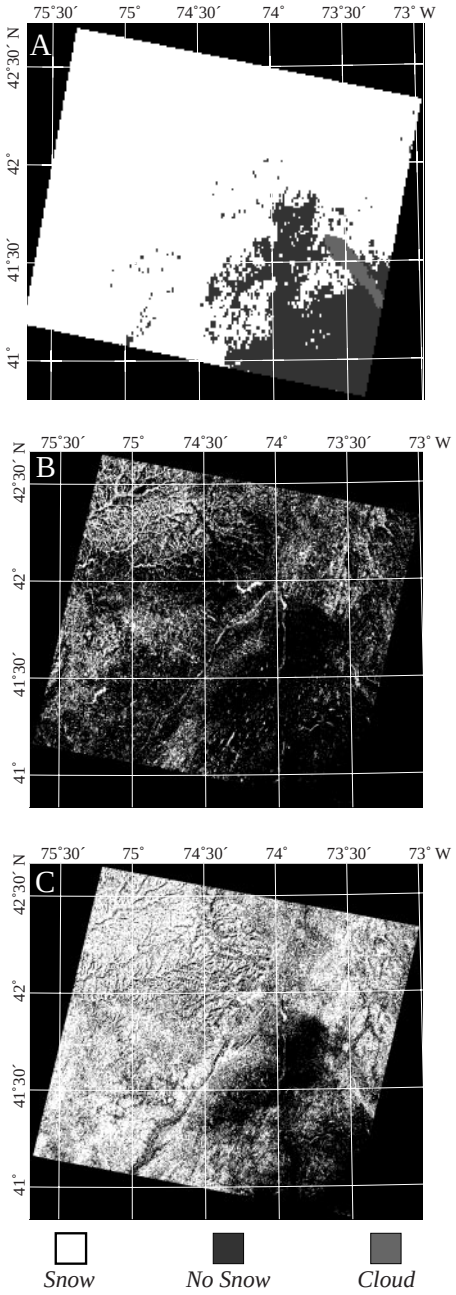
75°30´
75°
74°30´
74°
73°30´
73° W
42°30´ N
42°
41°30´
41°
A
B
C
Snow
No Snow
Cloud

Figure 6